OAK RIDGE NATIONAL LABORATORY LIBRARIES

3 4456 0545869 8

OAK RIDGE
NATIONAL LABORATORY

MANAGED BY UT-BATTELLE
FOR THE DEPARTMENT OF ENERGY

ORNL/TM-2003/213

Calculation of dpa Rates at the HFIR HB-2 Beam Tube Nozzle Corner Using Three-Dimensional Discrete Ordinates and Monte Carlo Models

June 2004

E. D. Blakeman
J. A. Bucholz
Oak Ridge National Laboratory

R. D. Cheverton
(Retired) Oak Ridge National Laboratory

UT-BATTELLE

ORNL-27 (2-03)

DOCUMENT AVAILABILITY

Reports produced after January 1, 1996, are generally available free via the U.S. Department of Energy (DOE) Information Bridge.

Web site http://www.osti.gov/bridge

Reports produced before January 1, 1996, may be purchased by members of the public from the following source.

National Technical Information Service
5285 Port Royal Road
Springfield, VA 22161
Telephone 703-605-6000 (1-800-553-6847)
TDD 703-487-4639
Fax 703-605-6900
E-mail info@ntis.fedworld.gov
Web site http://www.ntis.gov/support/ordernowabout.htm

Reports are available to DOE employees, DOE contractors, Energy Technology Data Exchange (ETDE) representatives, and International Nuclear Information System (INIS) representatives from the following source.

Office of Scientific and Technical Information
P.O. Box 62
Oak Ridge, TN 37831
Telephone 865-576-8401
Fax 865-576-5728
E-mail reports@adonis.osti.gov
Web site http://www.osti.gov/contact.html

This report was prepared as an account of work sponsored by an agency of the United States Government. Neither the United States Government nor any agency thereof, nor any of their employees, makes any warranty, express or implied, or assumes any legal liability or responsibility for the accuracy, completeness, or usefulness of any information, apparatus, product, or process disclosed, or represents that its use would not infringe privately owned rights. Reference herein to any specific commercial product, process, or service by trade name, trademark, manufacturer, or otherwise, does not necessarily constitute or imply its endorsement, recommendation, or favoring by the United States Government or any agency thereof. The views and opinions of authors expressed herein do not necessarily state or reflect those of the United States Government or any agency thereof.

ORNL/TM-2003/213

Nuclear Science and Technology Division (94)

Calculation of dpa Rates at the HFIR HB-2 Beam Tube Nozzle Corner Using Three-Dimensional Discrete Ordinates and Monte Carlo Models

E. D. Blakeman
J. A. Bucholz
Oak Ridge National Laboratory

R. D. Cheverton
(Retired) Oak Ridge National Laboratory

Date Published: June 2004

Prepared by the
OAK RIDGE NATIONAL LABORATORY
Oak Ridge, TN 37831-6285
Managed by
UT-BATTELLE, LLC,
for the
U.S. DEPARTMENT OF ENERGY
under contract DE-AC05-00OR22725

CONTENTS

LIST OF FIGURES v

LIST OF TABLES vii

ACKNOWLEDGMENTS ix

1. INTRODUCTION 1

2. CALCULATIONAL MODELS 5
   2.1 General Remarks 5
   2.2 Discrete Ordinates Models for the Core and Vessel Region 6
   2.3 3-D Discrete Ordinates Model of HB-2 8
   2.4 Core, Vessel Region, and Beam Tubes Monte Carlo Model 10

3. CALCULATIONAL RESULTS 15
   3.1 General Remarks 15
   3.2 Reactor Core Model Results 15
   3.3 Calculational Results for the HB-2 Beam Tube 15
   3.4 Summary of Results 21
   3.5 Discussion of Results 21
      3.5.1 Comparison of dpa rates at nozzle-corner positions 3:00 and 12:00 21
      3.5.2 Best estimate of dpa rate at nozzle corner 21

4. REFERENCES 23

APPENDIX A. VELM61 CROSS-SECTION SET AND GROUP STRUCTURE 25
APPENDIX B. 160-ANGLE X-AXIS STREAMING QUADRATURE 29
APPENDIX C. MODEL SUMMARY DATA ARCHIVE 33
APPENDIX D. FUEL REGION U-235 ATOM DENSITIES AND ZONE BOUNDARIES FOR DISCRETE ORDINATES AND MONTE CARLO CALCULATION MODELS 37
APPENDIX E. ISO-PLOTS OF DPA RATE CALCULATIONS 41

LIST OF FIGURES

Figure 1. Cross section of HFIR vessel and "core" showing locations of beam tubes, nozzles, and surveillance capsules (Keys 1-7)....2
Figure 2. Diagram of beryllium insert geometry for final design using actual vertical "strips" and "equivalent" annular design....3
Figure 3. HB-2 beam tube at vessel nozzle showing location of nozzle corner....4
Figure 4. Discrete ordinates 2-D model for the HFIR core and vessel....7
Figure 5. Discrete ordinates 3-D (TORT) model of HFIR HB-2, oriented to show main beam tube components....9
Figure 6. Discrete ordinates 3-D (TORT) model of HFIR HB-2, oriented to show beryllium insert....9
Figure 7. HFIR MCNP model showing plan view (horizontal cut) through reactor mid-plane....11
Figure 8. HFIR MCNP model showing HB-2 beam tube plan view (horizontal cut) close-up through reactor mid-plane with beam tube cross section through Be insert included....12
Figure 9. MCNP azimuthal detector locations at the nozzle corner for HB-2, showing detector number, "clock" analogy, and the global (X, Y, Z) coordinate ocations....13
Figure 10. Iso-plot of neutron dpa rate for HFIR HB-2 modified design for EOC conditions; plan view - horizontal cut along beam tube axis....16
Figure 11. Iso-plot of neutron dpa rate for HFIR JB-2 modified design for EOC conditions; elevation view – vertical cut along beam tube axis....16
Figure 12. Iso-plot of gamma dpa rate for HFIR HB-2 modified design for EOC conditions; plan view - horizontal cut along beam tube axis....17
Figure 13. Iso-plot of gamma dpa rate for HFIR HB-2 modified design for EOC conditions; elevation view – vertical cut along beam tube axis....17
Figure D.1. Schematic of HFIR fueled region boundaries for 2-D discrete ordinates model showing superimposed Monte Carlo cell boundaries....38
Figure D.2. Plot of U^{235} atom density for discrete ordinates and Monte Carlo models vs. radius for the HFIR inner fuel annulus....39
Figure D.3. Plot of U^{235} atom density for discrete ordinates and Monte Carlo models vs. radius for the HFIR outer fuel annulus....39
Figure E.1. Iso-plot of neutron dpa rate for HFIR HB-2 modified design for BOC conditions; plan view – horizontal cut along beam tube axis....42
Figure E.2. Iso-plot of neutron dpa rate for HFIR HB-2 modified design for BOC conditions; elevation view – vertical cut along beam tube axis....42
Figure E.3. Iso-plot of gamma dpa rate for HFIR HB-2 modified design for BOC conditions; plan view – horizontal cut along beam tube axis....43
Figure E.4. Iso-plot of gamma dpa rate for HFIR HB-2 modified design for BOC conditions; elevation view – vertical cut along beam tube axis....43
Figure E.5. Iso-plot of neutron dpa rate for HFIR HB-2 modified design for EOC conditions; annular beryllium insert; plan view – horizontal cut along beam tube axis....44
Figure E.6. Iso-plot of neutron dpa rate for HFIR HB-2 modified design for EOC conditions; annular beryllium insert; elevation view – vertical cut along beam tube axis....44
Figure E.7. Iso-plot of gamma dpa rate for HFIR HB-2 modified design for EOC conditions; annular beryllium insert; plan view – horizontal cut along beam tube axis....45
Figure E.8. Iso-plot of gamma dpa rate for HFIR HB-2 modified design for EOC conditions; annular beryllium insert; elevation view – vertical cut along beam tube axis....45
Figure E.9. Iso-plot of neutron dpa rate for HFIR HB-2 modified design for BOC conditions; annular beryllium insert; plan view – horizontal cut along beam tube axis....46
Figure E.10. Iso-plot of neutron dpa rate for HFIR HB-2 modified design for BOC conditions; annular beryllium insert; elevation view – vertical cut along beam tube axis....46
Figure E.11. Iso-plot of gamma dpa rate for HFIR HB-2 modified design for BOC conditions; annular beryllium insert; plan view – horizontal cut along beam tube axis....47
Figure E.12. Iso-plot of gamma dpa rate for HFIR HB-2 modified design for BOC conditions; annular beryllium insert; elevation view – vertical cut along beam tube axis....47
Figure E.13. Iso-plot of neutron dpa rate for HFIR HB-2 modified design for EOC conditions; no beryllium insert; plan view – horizontal cut along beam tube axis....48

Figure E.14. Iso-plot of neutron dpa rate for HFIR HB-2 modified design for EOC conditions; no beryllium insert; elevation view – vertical cut along beam tube axis.....48
Figure E.15. Iso-plot of gamma dpa rate for HFIR HB-2 modified design for EOC conditions; no beryllium insert; plan view – horizontal cut along beam tube axis.....49
Figure E.16. Iso-plot of gamma dpa rate for HFIR HB-2 modified design for EOC conditions; no beryllium insert; elevation view – vertical cut along beam tube axis.....49
Figure E.17. Iso-plot of neutron dpa rate for HFIR HB-2 modified design for BOC conditions; no beryllium insert; plan view – horizontal cut along beam tube axis.....50
Figure E.18. Iso-plot of neutron dpa rate for HFIR HB-2 modified design for BOC conditions; no beryllium insert; elevation view – vertical cut along beam tube axis.....50
Figure E.19. Iso-plot of gamma dpa rate for HFIR HB-2 modified design for BOC conditions; no beryllium insert; plan view – horizontal cut along beam tube axis.....51
Figure E.20. Iso-plot of gamma dpa rate for HFIR HB-2 modified design for BOC conditions; no beryllium insert; elevation view – vertical cut along beam tube axis.....51

LIST OF TABLES

Table 1. Summary of dpa rate calculations for HB-2 analysis using 3D discrete ordinates and MCNP models....18
Table 2. Summary of MCNP neutron dpa rate calculations for HB-2 3D analysis....19
Table 3. Comparison of dpa rate calculations at the HFIR nozzle corner for BOC and EOC conditions....20
Table 4. Comparison of dpa rate calculations at the HFIR nozzle corner with the Beryllium Insert Removed....20
Table A.1. VELM61 neutron group boundaries and iron dpa cross sections....26
Table A.2. VELM61 gamma group boundaries and iron dpa cross sections....27
Table B.1. 160-angle X-axis streaming quadrature....29
Table C.1. Equivalent TORT and MCNP runs for discrete ordinates and Monte Carlo model configuration....33
Table C.2. Auxiliary code sequence for discrete ordinates TORT runs....34
Table C.3. Computer hardware/software used for discrete ordinates and Monte Carlo analyses....35
Table E.1. Listing of Iso-plots for TORT dpa rate calculations....41

LIST OF TABLES

Table 1. Summary of dpa rate calculations for HB-2 analysis using 3D discrete ordinates and MCNP models.....18
Table 2. Summary of MCNP neutron dpa rate calculations for HB-2 3D analysis.....19
Table 3. Comparison of dpa rate calculations at the HFIR nozzle corner for BOC and EOC conditions.....20
Table 4. Comparison of dpa rate calculations at the HFIR nozzle corner with the Beryllium Insert Removed.....20
Table A.1. VELM61 neutron group boundaries and iron dpa cross sections.....26
Table A.2. VELM61 gamma group boundaries and iron dpa cross sections.....27
Table B.1. 160-angle X-axis streaming quadrature.....29
Table C.1. Equivalent TORT and MCNP runs for discrete ordinates and Monte Carlo model configuration.....33
Table C.2. Auxiliary code sequence for discrete ordinates TORT runs.....34
Table C.3. Computer hardware/software used for discrete ordinates and Monte Carlo analyses.....35
Table E.1. Listing of Iso-plots for TORT dpa rate calculations.....41

ACKNOWLEDGMENTS

The authors wish to thank the following persons for their help in this analysis: Igor Remec for supplying iron dpa cross sections in the VELM61 energy-group structure; J. V. Pace and L. R. Williams for generating the working VELM61 cross-section library and the HFIR core discrete ordinates model; J. C. Gehin and L. A. Smith for initial efforts in the development of the Monte Carlo HFIR model; and R. L. Childs for generating the directional quadrature set used in the three-dimensional discrete ordinates analysis. Appreciation is also extended to J. R. Inger for HFIR managerial support and to A. C. Alford for help in preparing the manuscript.

1. INTRODUCTION

The Oak Ridge National Laboratory (ORNL) High Flux Isotope Reactor (HFIR) has recently undergone an extensive upgrade, a part of which was to increase the diameters of two of the four radiation beam tubes, HB-2 and HB-4. These changes have increased the beam tube radiation streaming area and reduced the amount of water shielding at locations where the tubes penetrate the vessel wall. The result is that the neutron and gamma radiation dose rates, and thus radiation-induced embrittlement of the vessel wall near these locations, has been significantly increased. Radiation-induced embrittlement, which could ultimately result in a loss of integrity of the vessel wall, has been an ongoing issue of considerable interest and has been addressed in analyses related to vessel life-extension studies.[1-5]

In the more recent analyses of dpa rates,[4,5] calculations were performed for each of the HFIR beam tubes for configurations before and after modifications. The damage parameter used in these evaluations is displacements/atom (dpa) in iron (the major constituent in the vessel wall) that result from neutron and gamma radiation. Calculated dpa rates (i.e. displacements/atom/s) obtained from these calculations were incorporated into statistical damage evaluation studies and the subsequent analyses have been reported.[3] This report presents the results of updated dpa analyses for HB-2. As shown in Figure 1, HB-2 is aligned with a radial vector from the reactor core; that is, the axis of HB-2 passes through the vertical centerline of the reactor core. For this reason, and considering the state-of-the-art in 1986, a judgment was made at that time that a two-dimensional (2-D) analysis of the dose rates in the pressure vessel in the vicinity of the HB-2 nozzle was adequate,[1] whereas the other beam lines, which lack the required symmetry, required a more complicated and computationally-intensive three-dimensional (3-D) model. The 2-D model for HB-2 was also considered appropriate for the later vessel life-extension studies that eventually included the new (larger-diameter) HB-2 beam tube.[3,4,5] For this latter analysis, the beryllium insert in the tip of the beam tube thimble (Figure 2) was modeled as a cylindrical annulus that feathered into the hemispherical end of the beam tube thimble. This simplification of the insert geometry was appropriate for the life-extension feasibility studies,[3] but it was recognized that the use of a 3-D model could result in a shorter specified time between hydro tests sometime later in the life of the vessel. Thus, it was recommended that a 3-D analysis be performed in the near future. Analyses reported herein are in fulfillment of that recommendation.

In the previously reported analyses,[4,5] dpa rates for beam tubes HB-2,-3, and -4 were calculated using a discrete ordinates neutronics calculation methodology. For the present study both a 3-D discrete ordinates model and an existing Monte Carlo model, modified to incorporate the enlarged HB-2 beam tube, were used. The Monte Carlo analysis was included for comparison purposes.

As indicated in Figure 1, the beam tubes enter/exit the vessel through the nozzles. The nozzle corners (Figure 3), because of their proximity to the beam tubes, are subjected to relatively high dpa rates, and for other reasons are also subjected to relatively high stresses.[1-3] Thus, the HB-2 nozzle corner is of particular interest with regard to vessel integrity, and in this study the comparison of results obtained with the various models is made at this location. Even so, the discrete-ordinates analysis provides dpa rate values throughout the entire geometric model.

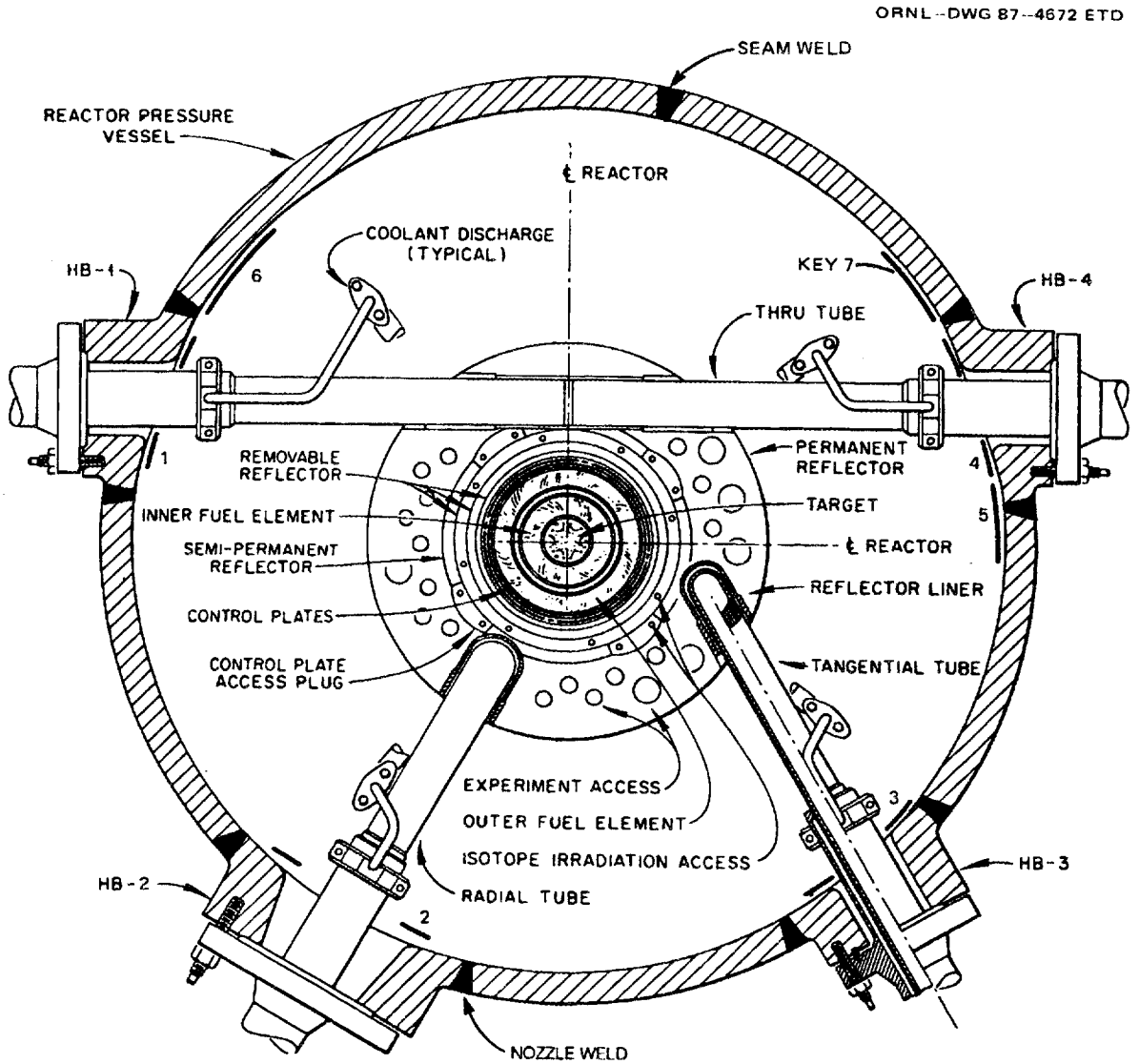

Figure 1. Cross-section of HFIR vessel and "core" showing locations of beam tubes, nozzles, and surveillance capsules (Keys 1 – 7).

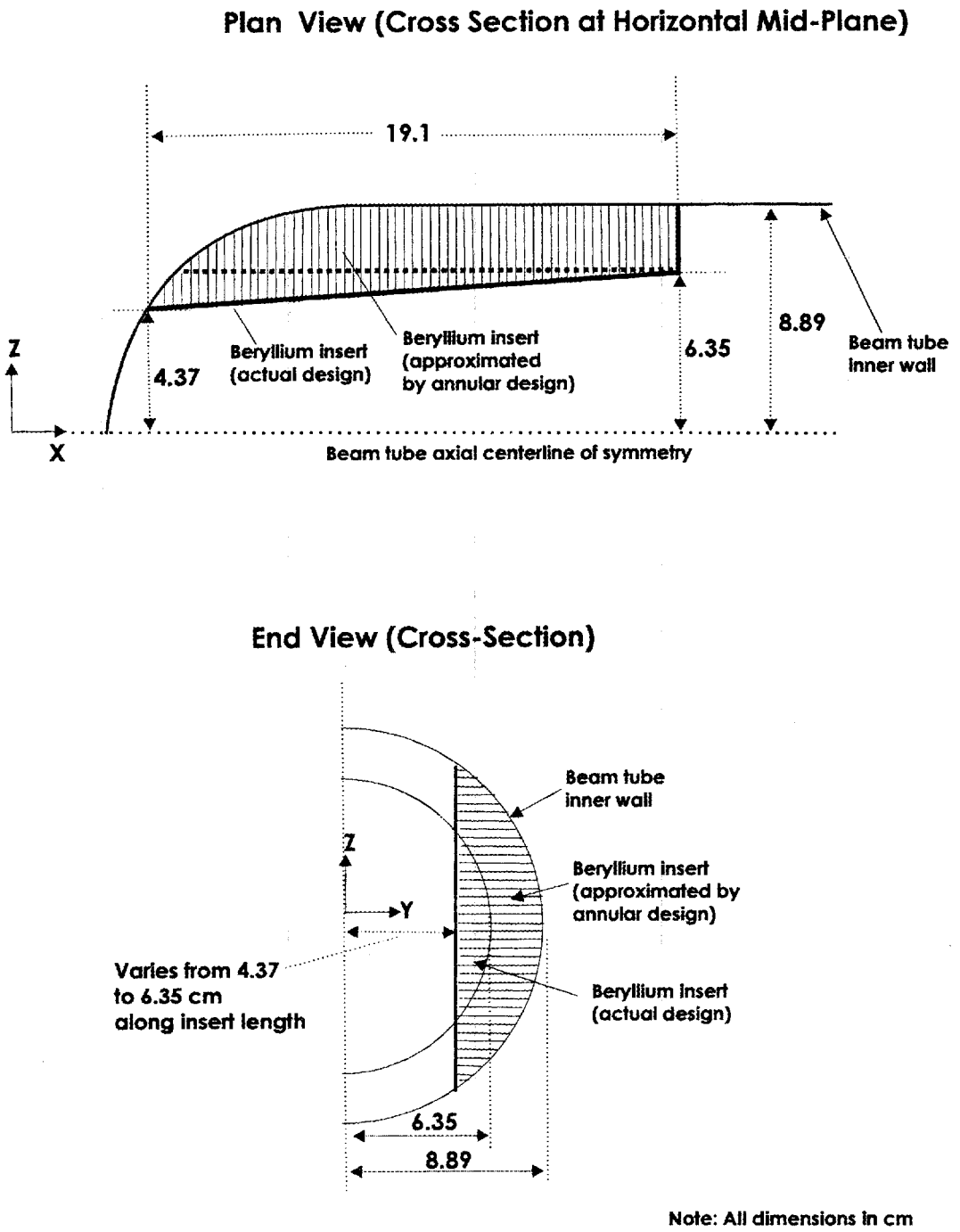

Figure 2. Diagram of beryllium insert geometry for final design using actual vertical "strips" and "equivalent" annular design.

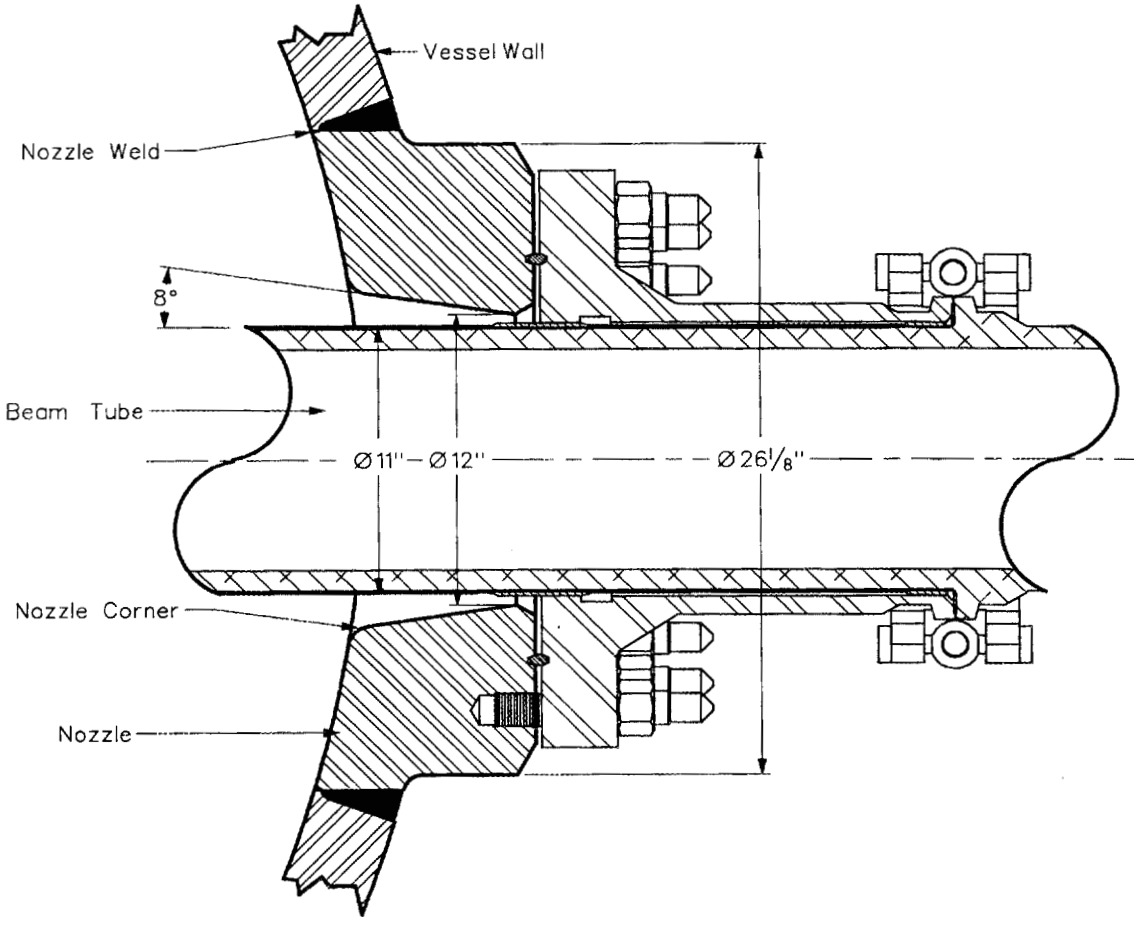

Figure 3. HB-2 beam tube at vessel nozzle showing location of nozzle corner.

2. CALCULATIONAL MODELS

2.1 GENERAL REMARKS

Discrete ordinates calculations for these analyses were performed using either 2-D or 3-D models utilizing the DORT[6] and TORT[7] 2-D and 3-D codes from the DOORS[8] transport code system developed at ORNL and distributed by the ORNL Radiation Safety Information Computational Center (RSICC).

The calculations were performed using the VELM61[9] broad-group cross-section library. Neutron and gamma dpa cross-section values[10,11] were converted to the VELM61 energy group structure. Appendix A, Table A.1, shows the VELM61 cross-section energy group structure and the corresponding dpa response cross section for each group.

Calculations were performed using P_3 scattering cross sections and a quadrature order of at least S_{10}, both of which have been shown from earlier analyses[4,5] to be adequate for these cases. A special "streaming" quadrature was used for the TORT calculations and is listed in Appendix B. Also, an additional assessment[12] was made earlier to justify the use of P_3 scattering cross sections instead of the more computationally demanding P_5 scattering cross sections. The expansion order determines the degree of scattering anisotropy, and the quadrature order determines angular resolution.

Neutron and gamma sources for the HB-2 beam tube discrete ordinates calculations were obtained from fixed-source calculations of the HFIR core utilizing beginning-of-cycle (BOC) fuel conditions, and with control plates in either the end-of-cycle (EOC) or BOC location. Thus, for the discrete ordinates calculations, the term "EOC" refers to the location of the control plates only, since the more reactive BOC fuel was always used. This approach was adopted in the earlier calculations, at which time it was considered convenient and conservative. In all cases, the reactor power was normalized to the same power level (100 MW).

The discrete ordinates calculation involved a multi-step process. The first step was to perform a 2-D cylindrical (RZ) calculation of the HFIR core to obtain a 2-D distribution of the fission source in the fuel. This source was then used in a second, enlarged 2-D cylindrical reactor model that included the vessel and the surrounding water. (Details of these calculations are provided in Section 2.2.) The neutron and gamma directional flux distributions from this latter model were then used to create a boundary source for the 3-D beam tube model. This conversion was performed using the auxiliary codes, VISA and TORSED, also from the DOORS system. This procedure is discussed in somewhat more detail in the report on the earlier discrete ordinates beam tube analysis.[4] (Appendix C, which addresses the archive of calculational models and data, provides a more detailed summary of the calculational sequence.) This boundary source was then used as input to the 3-D TORT model of HB-2, which is discussed in detail in Section 2.3.

Additional and completely independent calculations employing the MCNP[13] Monte Carlo code were also performed for BOC and EOC conditions. The model for these calculations explicitly included the reactor core and the beam tubes. It is discussed further in Section 2.4.

Compositions of the fuel, water, and structural materials used in the discrete ordinates calculations were previously reported in Appendix C of Reference 4 and are not repeated here. However, it is of interest to provide some additional information on the fuel compositions for the discrete ordinates and Monte Carlo models. Fuel regions and BOC atom densities for the Monte Carlo model were derived from, and are nearly identical to, those of an early core design analysis,[14] whereas those for the discrete ordinates analysis were obtained from a newer, revised analysis.[15] Appendix D shows a comparison of both models

in the fuel region and shows that the two models, for the purpose of the present calculations, are essentially equivalent.

2.2 DISCRETE ORDINATES MODELS FOR THE CORE AND VESSEL REGION

As discussed in Section 2.1, 2-D cylindrical (RZ) calculations of the HFIR core were performed to obtain a source for the subsequent 3-D beam tube calculations. For these calculations, the HFIR reactor was modeled in a 2-D cylindrical (RZ) geometry using the DORT 2-D transport code. The beam tubes were omitted in this model. The reactor calculations were then performed in two steps. First, an eigenvalue (k_{eff}) calculation for the reactor core was performed using a model that was limited in the radial direction to a distance of 25 cm into the water beyond the outer edge of the beryllium reflector (which was neutronically equivalent to an infinite water reflector beyond the beryllium reflector). The calculated fission source was subsequently input as a fixed source in an expanded model that extended 30.48 cm (12 in.) beyond the vessel wall. The source strength was normalized to the HFIR maximum operating power level of 100 MW (which corresponds to a volume-integrated neutron source of 7.557×10^{18} s^{-1} in the core). Figure 4 shows the reactor core fixed-source geometry model. Note that there are two water regions in the vessel, beyond the beryllium reflector. The boundary between the two regions is the outer boundary for the k_{eff} reactor core model.

The fuel region and its composition are further described in Appendix D.

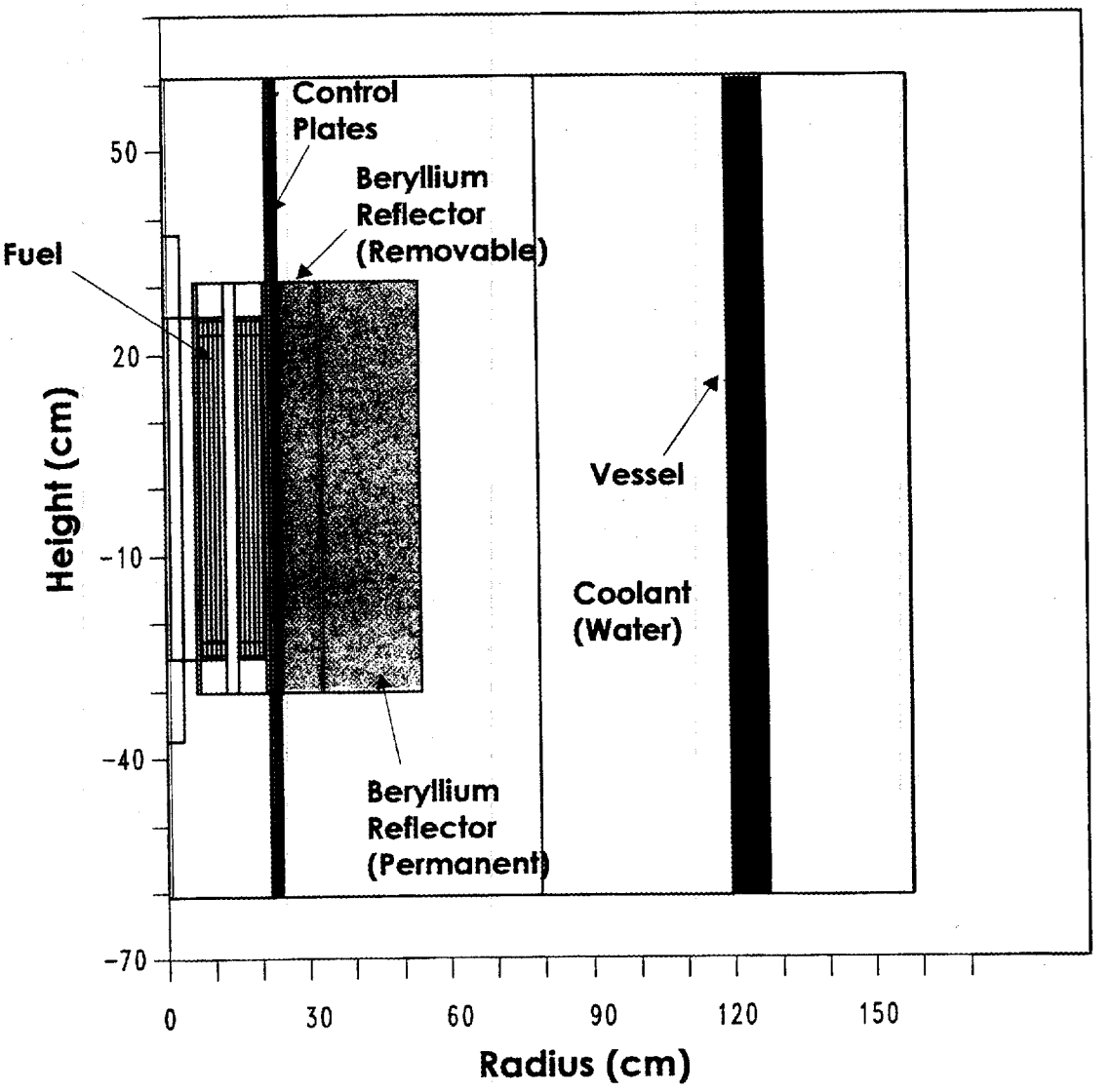

Figure 4. Discrete ordinates 2-D model for the HFIR core and vessel.

2.3 3-D DISCRETE ORDINATES MODEL OF HB-2

The HB-2 TORT 3-D geometry model consists of a portion or the core/vessel assembly that includes the HB-2 beam tube to a radial position outside the vessel; a beryllium insert in the innermost end of the beam tubes; portions of the surrounding beryllium and water reflectors, vessel wall, and nozzle; and a mount for dosimeters and vessel material surveillance capsules. As discussed in Section 2.2, calculations of the reactor without the beam tubes are made to obtain neutron and gamma sources that are applied to the enveloping surface of this core/vessel "cell" in preparation for the calculation of the neutron and gamma fluxes and dpa rates inside the cell. The surface of the cell is sufficiently removed from the beam tube that source terms are minimally affected by the presence of the beam tubes.

The specific 3-D discrete ordinates geometry based on the TORT code is shown in Figures 5 and 6. Coordinate axes for the model are oriented so that the x-axis is along the beam tube center line with the positive direction being away from the reactor core toward the vessel wall, and the z-axis being in the upward (vertical) direction. Figure 6 is an approximate horizontal cut through the core mid-plane, which shows a view of the beryllium insert not visible in Figure 5. Note that all curved surfaces have a "stair-cased" appearance since the model is constructed exclusively from rectangular solid boxes (also referred to as "bodies").

A diagram of the beryllium insert was shown in Figure 2. Geometrically, the insert consists of two vertical "strips" located on each side of the beam tube and feathered into the beam tube walls. As is also shown, the beam tube opening along the length of the insert increases in area as the insert becomes thinner. Figure 2 also shows a diagram of the 2-D annular approximation to the insert that encircles the inside of the beam tube and feathers into the beam tube tip. Note that in Figure 5 the beryllium insert cannot be seen, since the vertical cut shown is along the plane through the center of the beam tube. The model shown in Figures 5 and 6 is a cutaway view of the actual calculation model; only the positive half of the Y-axis is shown. The base-case model comprises 402 rectangular solid bodies. The calculation model is divided into 87, 132, and 39 mesh intervals in the X,Y, and Z directions respectively. There are, as a result, 447,876 mesh cells. The angular quadrature set used is a 160-direction set tailored for particle streaming along the X-axis and is listed in Appendix B.

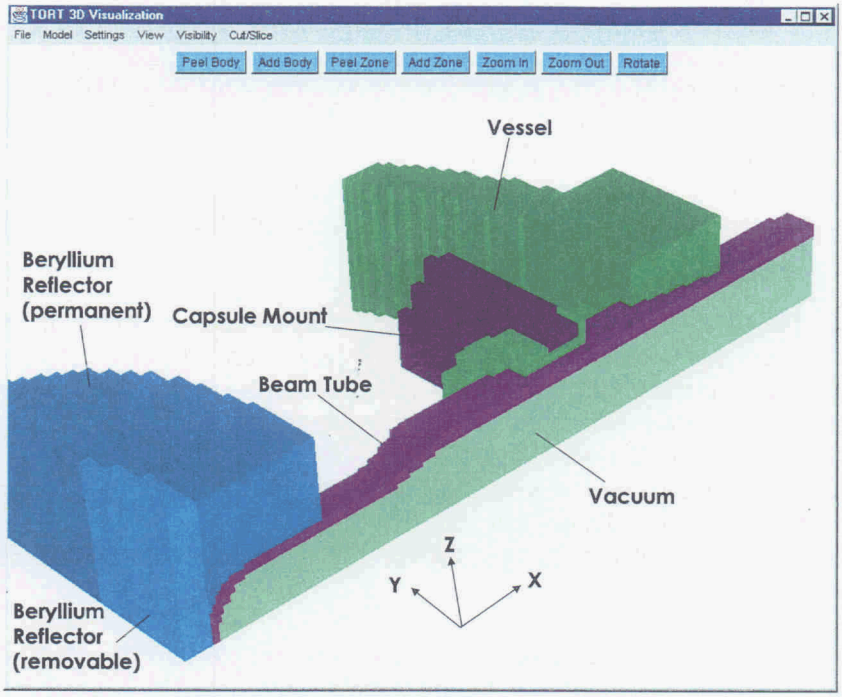

Figure 5. Discrete ordinates 3-D (TORT) model of HFIR HB-2, oriented to show main beam tube components.

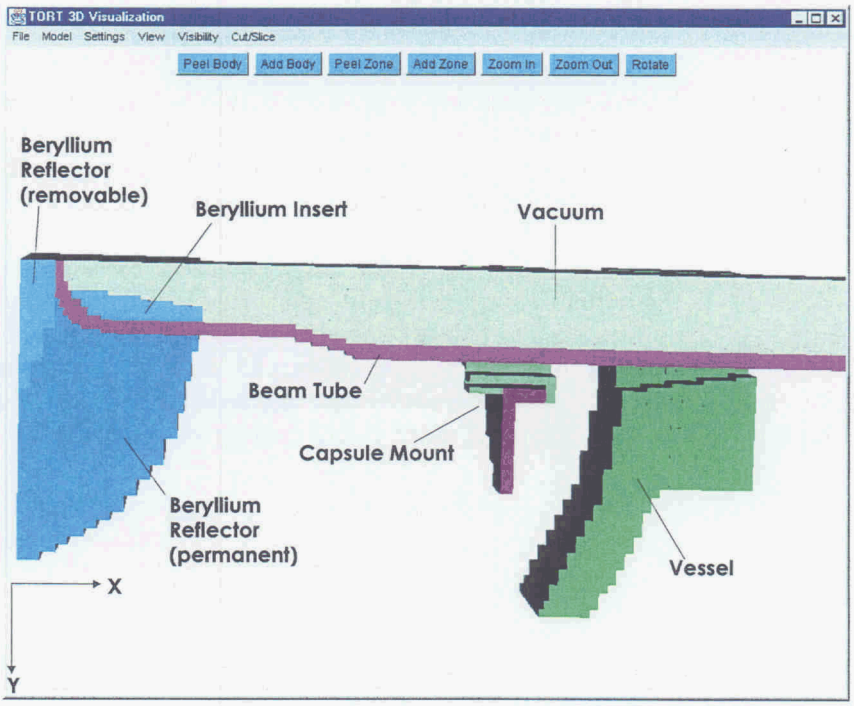

Figure 6. Discrete ordinates 3-D (TORT) model of HFIR HB-2, oriented to show beryllium insert.

2.4 CORE, VESSEL REGION, AND BEAM TUBES MONTE CARLO MODEL

Additional calculations were performed using the MCNP Monte Carlo code. The model employed in these calculations was a modification of an existing HFIR Monte Carlo model developed over a multi-year period and used extensively in other HFIR analyses.[16] Figure 7 shows a horizontal view of the model at the reactor mid-plane. Figure 8 shows a detailed view of HB-2 and the beryllium insert inside the beam tube. The model also contains details of the beam lines well beyond the reactor vessel and not shown in Figures 7 and 8.

The approach using MCNP for these analyses was considerably different from the discrete ordinates method described earlier. The Monte Carlo calculations were performed using an "all-inclusive" model that includes the reactor core and all beam tubes. The source for the model comprises fission densities distributed over the core that were determined by k_{eff} calculations. A standard Watt neutron-energy spectrum for ^{235}U was used. All detector response tallies were normalized to a power level of 100 MW. This corresponded to a volume-integrated source strength of 7.5573×10^{18} s^{-1} in the core, which is the same as that used for the discrete ordinates calculations. As stated earlier, material compositions were obtained from Reference 14, which predates and differs slightly from those used (Reference 15) in the discrete ordinates models.

Neutron fluxes and dpa rates were calculated using a ring of point detector tallies located at the exit of the beam tube at the nozzle corner (cf. Figure 8). Figure 9 shows the azimuthal locations of the eight detectors used. Detectors were spaced at 45° increments and can be referenced by their equivalence to a "clock" position, e.g. 12:00 for a position directly above the beam line and 3:00 or 9:00 for positions on the reactor mid-plane. For each detector, the (X,Y,Z) coordinates with respect to the reactor core center are given. It should be noted that for the MCNP model, the direction along the beam tube toward the vessel wall was assigned to the negative X-axis. For the discrete ordinates model, however, this direction was the positive X-axis.

The MCNP model includes multiple beam tubes; however, since only HB-2 was of interest, a DXTRAN sphere was located around the HB-2 detectors at the beam tube nozzle (cf. Figure 7). This is an MCNP variance reduction mechanism whereby "pseudo-particles" are generated at particle collision sites and transported to the sphere. As a result, calculational precision is increased at the detector locations within the sphere.

For the MCNP model, fuel configurations, control positions, and sources were determined for BOC and EOC conditions. EOC fuel conditions were calculated[17] using a modification of the model employed in the VENTURE[18] diffusion theory analysis presented in Reference 15. In addition, calculations were performed with EOC control positions but with the source and fuel configured for BOC conditions in order to provide a basis of comparison with some of the discrete ordinates calculations.

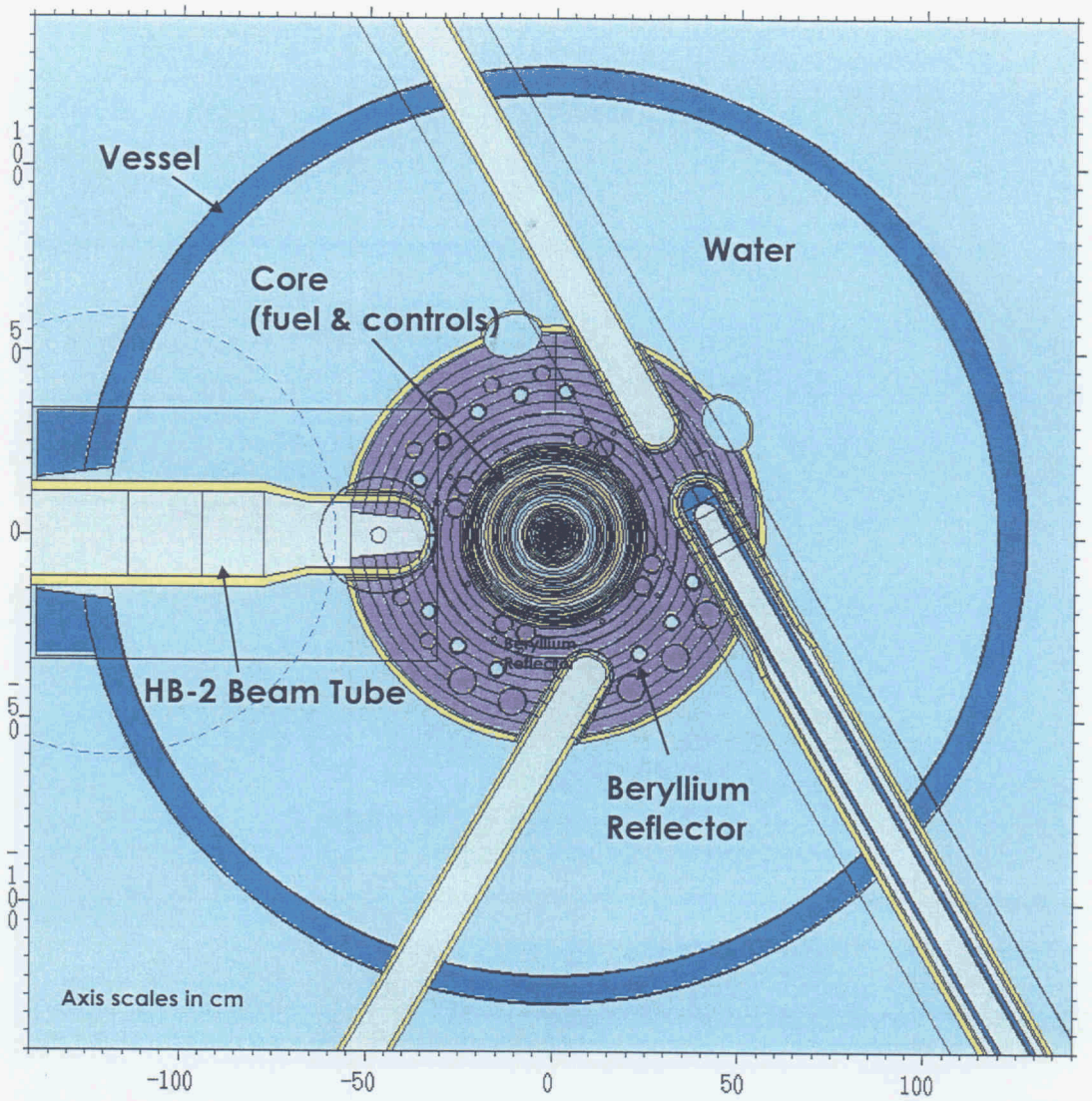

Figure 7. HFIR MCNP model showing plan view (horizontal cut) through reactor mid-plane.

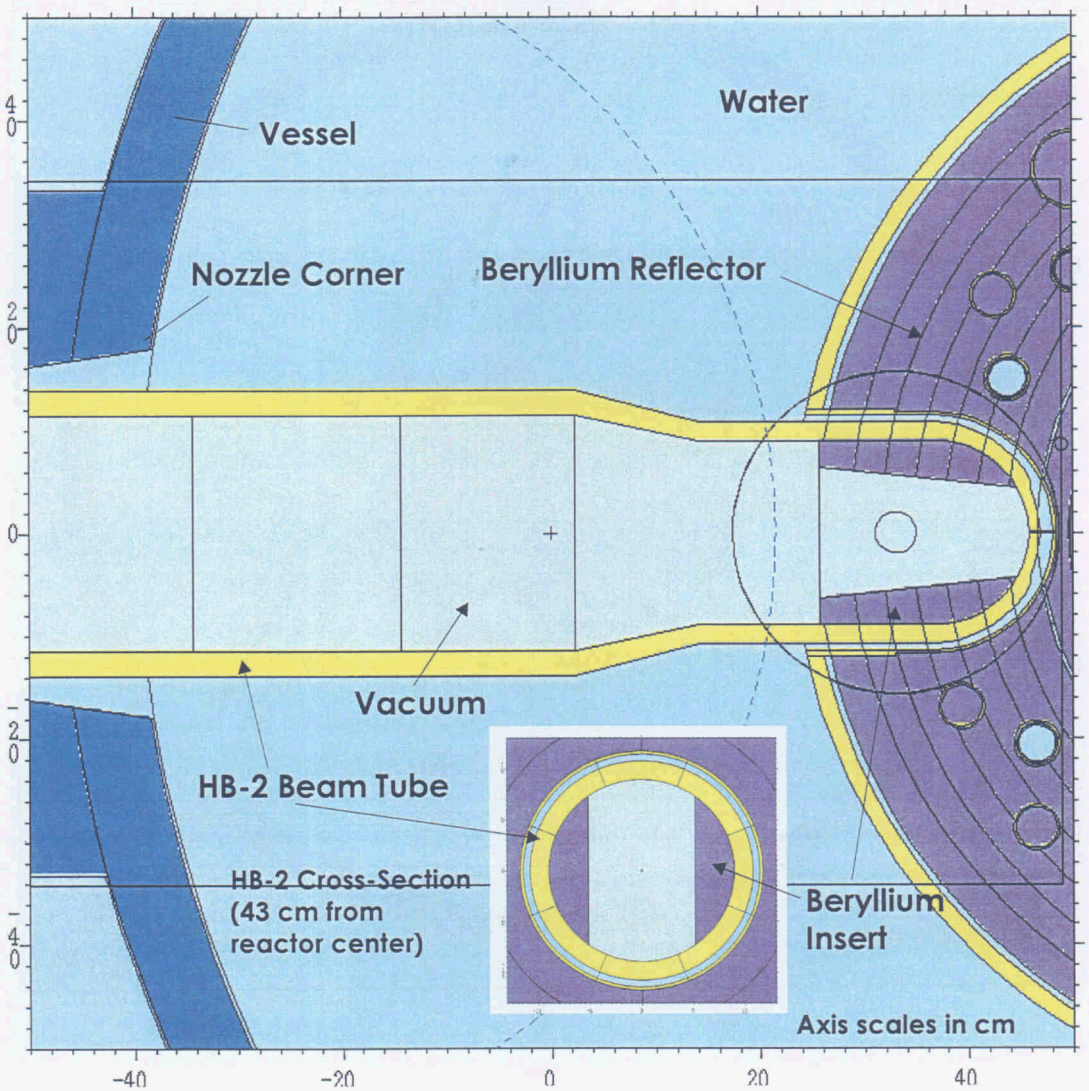

Figure 8. HFIR MCNP model showing HB-2 beam tube plan view (horizontal cut) close-up through reactor mid-plane with beam tube cross section through Be insert included.

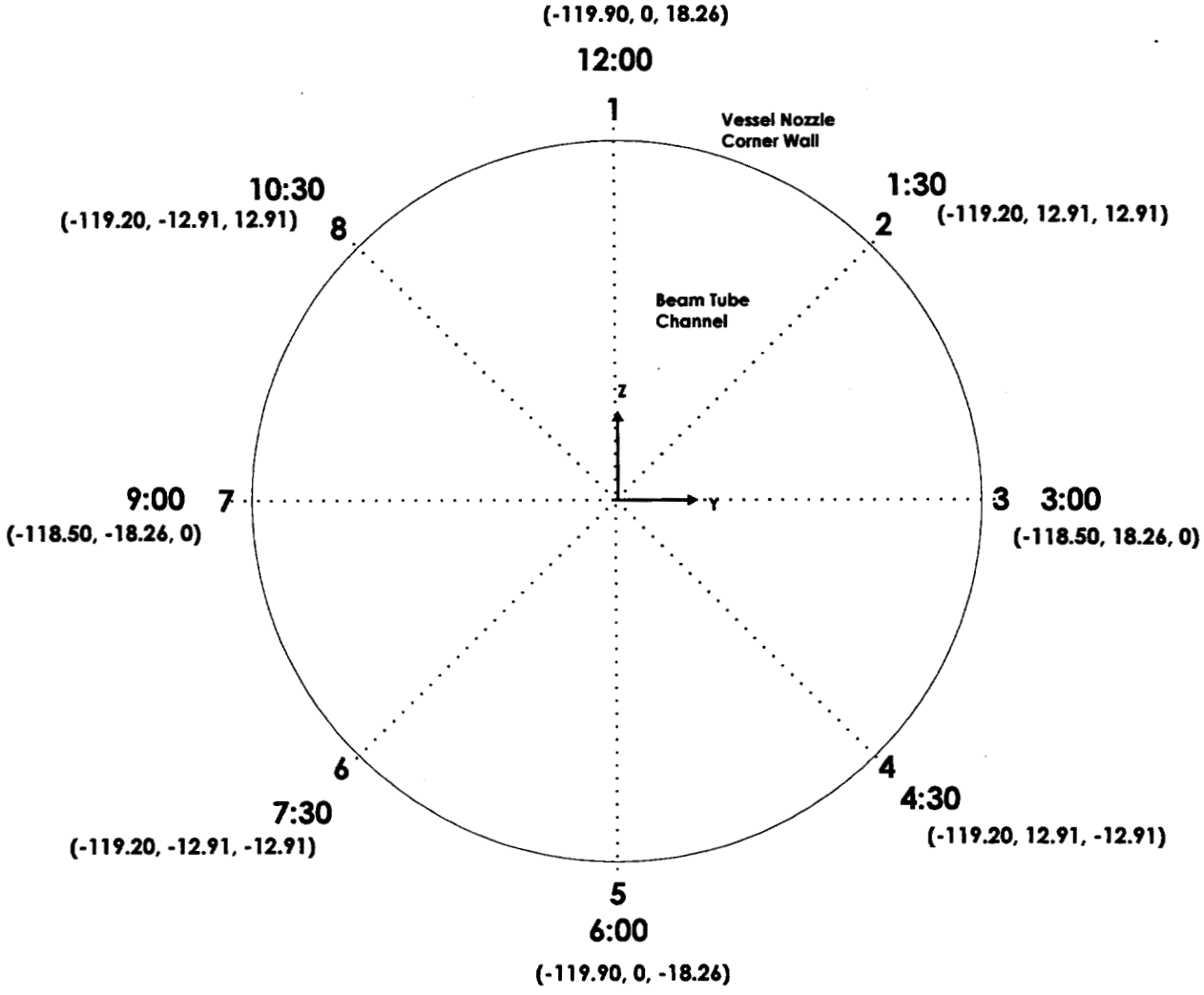

Figure 9. MCNP azimuthal detector locations at the nozzle corner for HB-2, showing detector number, "clock" analogy, and the global (X,Y,Z) coordinate locations. Orientation is such that the reader is looking in the -X direction along the beam tube axis away from the reactor core.

3. CALCULATIONAL RESULTS

3.1 GENERAL REMARKS

The particular results of interest were the dpa rates at locations on the HB-2 nozzle corner. The dpa rate is determined by folding the neutron or gamma flux with the energy-dependent iron dpa cross sections and integrating over the complete energy spectrum. In discrete ordinates calculations the flux, and thus the dpa rate, is calculated everywhere in the model. It should be clear, however, that the dpa rate has absolute relevance only at locations where iron is present, e.g. the vessel wall. Otherwise, plotted dpa rate values are similar in appearance to plots of fast flux and serve as an indicator of flux trends. In contrast, Monte Carlo results are obtained only at specified locations corresponding, in this case, to points around the nozzle corner.

3.2 REACTOR CORE MODEL RESULTS

Reactor core calculations are discussed in detail in an earlier report.[4] Similar calculations were used for this analysis. Calculations in the previous analysis used an S_{10} symmetric angular quadrature. This led to some concern since the gamma dpa rate exhibited "ray effects," a non-physical phenomenon attributed to an insufficient number of quadrature angles in which particle densities are enhanced along angular directions. The original S_{10} results were later judged to be adequate only after follow-up calculations using an S_{16} quadrature resulted in a gamma dpa rate difference of only ~1% in the regions of interest. Still, even though the difference was small, the S_{16} quadrature was used for the reactor core calculations in this new analysis, thereby eliminating any lingering concerns over the quadrature.

3.3 CALCULATIONAL RESULTS FOR THE HB-2 BEAM TUBE

Figures 10 through 13 show iso-plots of the TORT results for the neutron and gamma dpa rates for the "base-case" discrete ordinates EOC calculations. (The prefix "iso-" is used to refer to equal-value contour lines in these plots and is used with the quantity of interest, i.e. iso-dpa rate.) Plots for additional calculations discussed in this section are shown in Appendix E. The plots demonstrate the high degree of neutron streaming occurring within the beam tube void. Results from the discrete ordinates (TORT) and the Monte Carlo (MCNP) calculations are both summarized in Table 1. The MCNP runs typically used 320 million histories to achieve the listed statistics. Cases were also run in which the beryllium insert was represented as an annulus in an effort to duplicate and compare with the 2-D calculation. For this situation, the beryllium insert geometry was simplified and modeled as a 2.54-cm-thick annulus, which is the same as the model used in the earlier 2-D discrete ordinates cases. In this case, the calculations with the annular beryllium model did not include the "flaring" effect present in the actual design (which had been included in the more rigorous 3-D models).

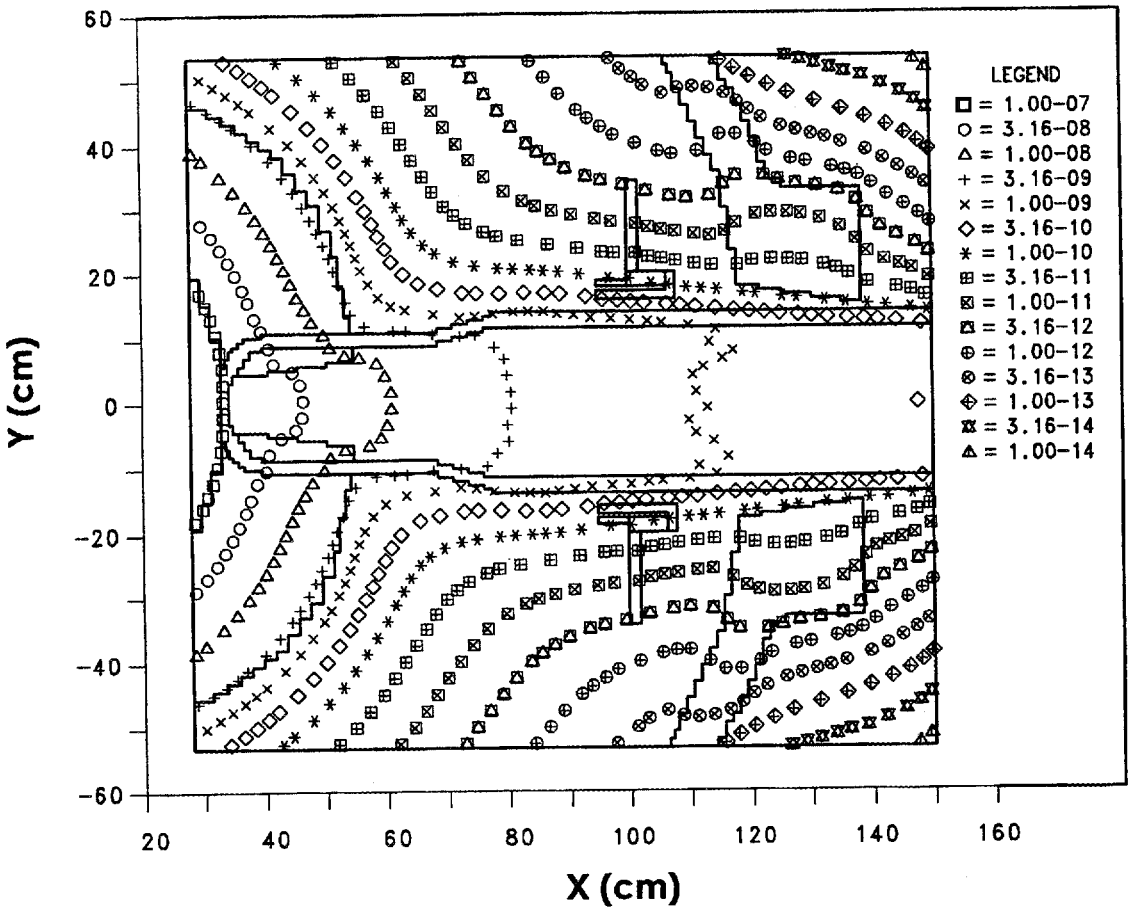

Figure 10. Iso-plot of neutron dpa rate for HFIR HB-2 modified design for EOC conditions; plan view — horizontal cut along beam tube axis.

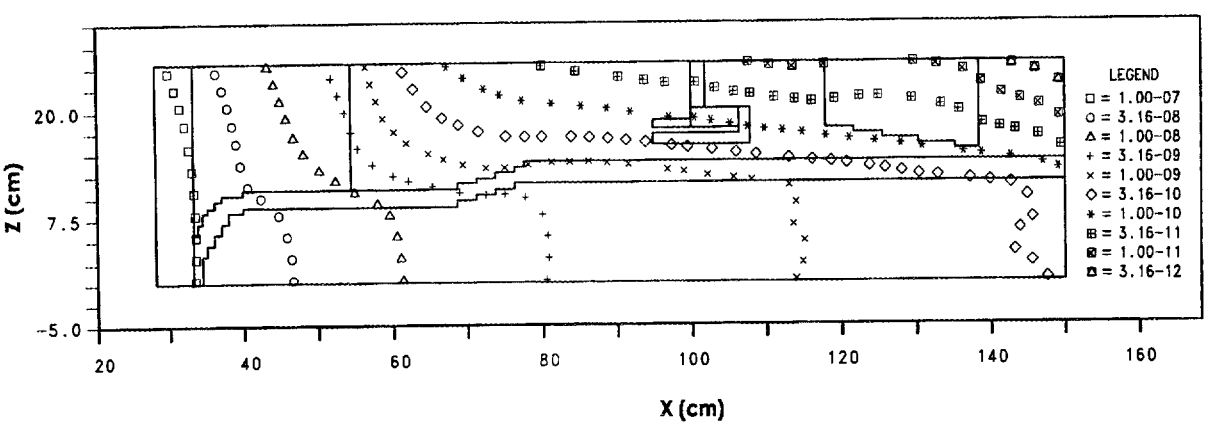

Figure 11. Iso-plot of neutron dpa rate for HFIR HB-2 modified design for EOC conditions; elevation view — vertical cut along beam tube axis.

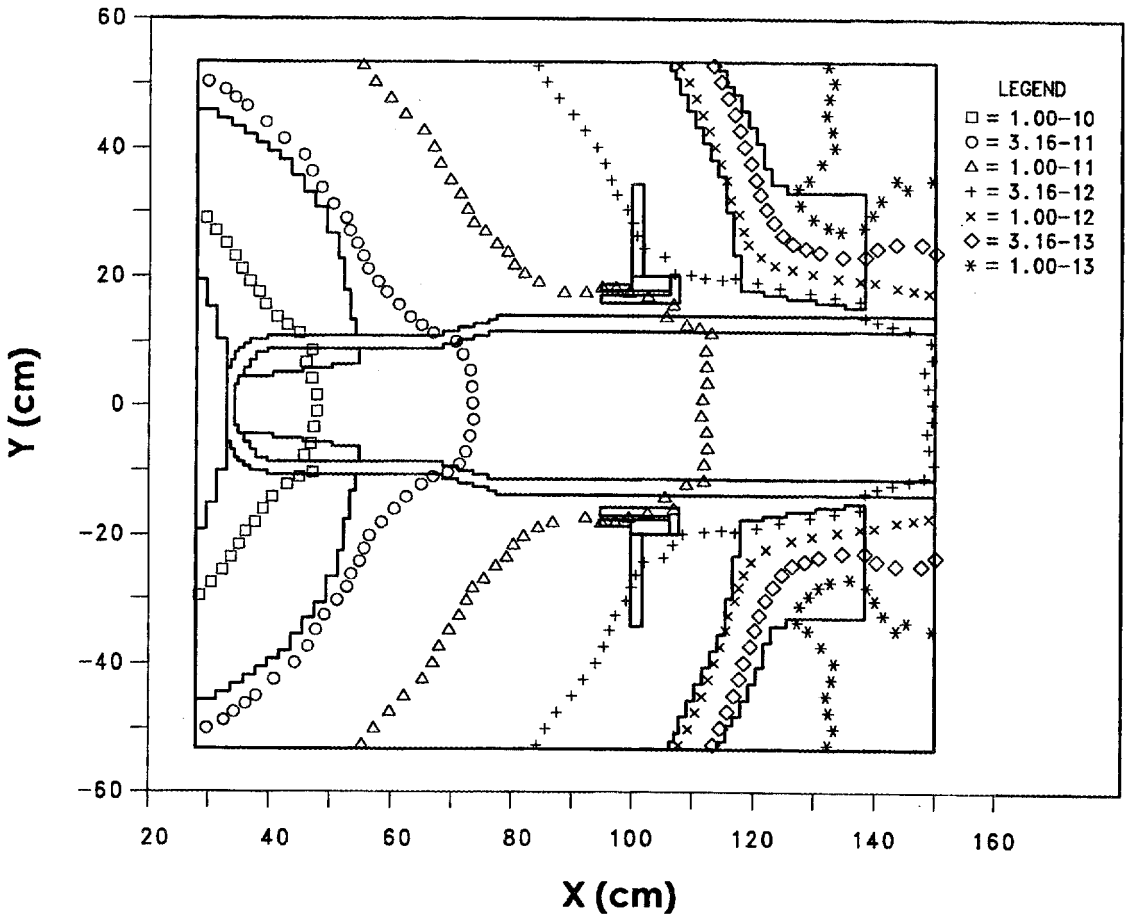

Figure 12. Iso-plot of gamma dpa rate for HFIR HB-2 modified design for EOC conditions; plan view — horizontal cut along beam tube axis.

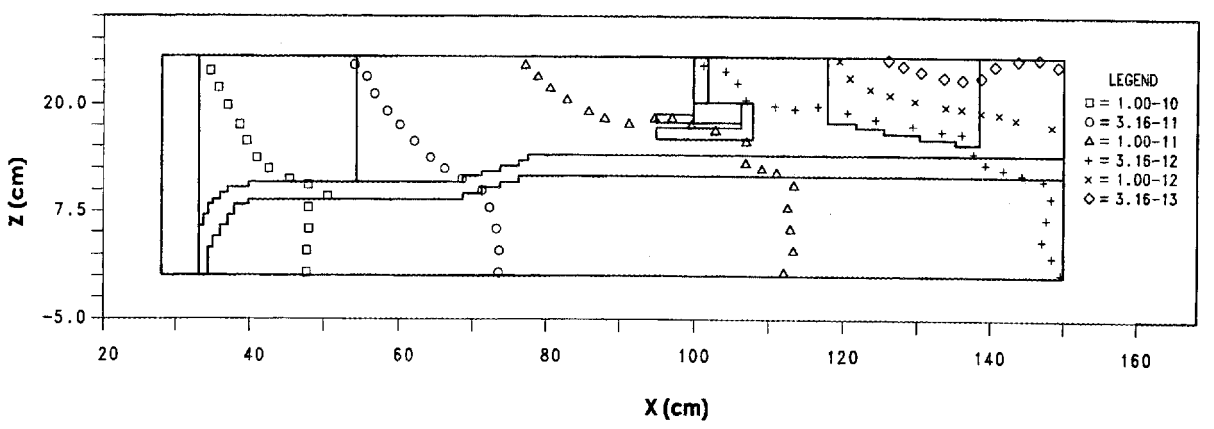

Figure 13. Iso-plot of gamma dpa rate for HFIR HB-2 modified design for EOC conditions; elevation view — vertical cut along beam tube axis.

Table 1. Summary of dpa rate calculations for HB-2 analysis using 3-D discrete ordinates and MCNP models

Model type	Run ID[a]	BOC/ EOC?	Beryllium insert[b]	Corner position	dpa rate (10^{-12} s^{-1})		
					Neutron	Gamma	Total
Discrete ordinates (2-D)	1	EOC[c]	Annulus	N/A	57.0	3.80	60.0
Discrete ordinates (3-D)	3	EOC[c]	Strips	3:00	63.6	4.34	67.9
				12:00	61.0	4.12	65.1
	7	BOC	Strips	3:00	59.9	3.57	63.5
				12:00	57.7	3.40	61.1
	4	EOC[c]	Annulus	3:00	53.0	3.76	56.8
				12:00	52.2	3.59	55.8
	11	BOC	Annulus	3:00	50.0	3.10	53.1
				12:00	49.5	2.96	52.5
Monte Carlo (3-D)	A	EOC	Strips	3:00	55.1 (7)[d]	-----	-----
				12:00	51.8 (5)	-----	-----
	G	EOC[c]	Strips	3:00	47.5 (5)	-----	-----
				12:00	45.6 (4)	-----	-----
	B	BOC	Strips	3:00	45.1 (5)	-----	-----
				12:00	41.1 (4)	-----	-----
	E	EOC	Annulus	3:00	46.2 (5)[e]	-----	-----
				12:00	39.7 (3)	-----	-----
	F	BOC	Annulus	3:00	37.6 (5)	-----	-----
				12:00	35.2 (3)	-----	-----

[a]Number/letter refers to partial name of TORT or MCNP run. See description of models in Appendix C.
[b]Beryllium "strips" refers to the "as designed" insert comprising of two separate vertical strips that line the inside of the beam tube. "Annulus" refers to a simplified annular insert that simulates the 2-D approach.
[c]Control plates are in EOC position, but fuel composition corresponds to BOC.
[d]Value in parentheses is Monte Carlo fractional standard deviation expressed as a percent.
[e]The equivalent 9:00 position is given instead of the 3:00 position because of better precision obtained.

Additional MCNP model results are given in Table 2, which includes results of dpa rate calculations at all eight detector positions at the HB-2 nozzle corner. Table 3 shows a comparison between equivalent TORT and MCNP dpa rate calculations. Since the MCNP results do not extend to energies below 27 keV, the TORT values for energies above 27 keV are given along with the total dpa rates summed over all energies. The thermal group dpa rate is included separately. Two conclusions are evident with regard to the TORT calculations: (1) the dpa rate for energies above 27 keV accounts for ~90% of the total dpa rate, and (2) the thermal dpa rate accounts for almost all of the dpa rate for energies below 27 keV. Care has been taken in Table 3 not to directly compare the EOC TORT calculations with the EOC MCNP calculations, since the TORT EOC calculations were performed with BOC fuel conditions. Instead, an MCNP calculation was performed with similar conditions, i.e. BOC fuel and EOC control conditions, in order to provide a basis of comparison.

Additional TORT and MCNP calculations were performed with the beryllium insert removed. The purpose of these calculations was to determine the overall effect of the insert, to further evaluate the variation in dpa rate for different locations around the nozzle corner, and to provide additional comparisons between the discrete ordinates and Monte Carlo calculation methodologies. Table 4 shows the results.

Table 2. Summary of MCNP neutron dpa rate calculations for HB-2 3D analysis

Description	**MCNP runs for EOC/BOC conditions using different beryllium insert configurations**				
Run ID[a] **histories (x10^6)** **EOC/BOC?** **Be insert**[c]	A 320 EOC strips	G 320 EOC[b] strips	B 320 BOC strips	E 320 EOC annulus	F 320 BOC annulus
Detector locations	**Detector dpa rates (x 10^{-12} s-1)**				
1 (12:00)	50.3 (4)[d]	45.6 (4)	42.8 (4)	39.7 (3)	35.2 (3)
2 (1:30)	48.7 (5)	46.7 (5)	48.4 (12)	40.3 (3)	41.0 (6)
3 (3:00)	56.9 (11)	47.5 (5)	44.3 (4)	48.2 (12)	37.6 (5)
4 (4:30)	53.3 (10)	44.0 (4)	56.5 (16)	39.2 (3)	36.4 (4)
5 (6:00)	53.2 (5)	43.7 (3)	39.5 (2)	43.2 (7)	37.2 (5)
6 (7:30)	50.5 (4)	48.8 (6)	43.3 (3)	47.0 (12)	36.5 (4)
7 (9:00)	53.2 (5)	50.9 (7)	50.0 (6)	46.2 (5)	39.2 (8)
8 (10:30)	52.3 (5)	49.5 (12)	43.6 (3)	44.0 (4)	39.4 (6)

[a]Letter refers to partial name of run. Full name of run is, e.g., hf245Ah, where hf245 indicates base case configuration; and final letter designation, e.g., h, indicates number of histories. See description of models in Appendix C.
[b]EOC control position but BOC fuel.
[c]Options are (1) vertical Be strips as designed; (2) Be annulus representing simplified 2-D simulation.
[d]Value in parentheses is Monte Carlo fractional standard deviation expressed as a percentage.

Table 3. Comparison of dpa rate calculations at the HFIR nozzle corner for BOC and EOC conditions

Run ID		EOC/	Nozzle	Neutron dpa rate (x 10^{-12} s^{-1})				MCNP/
			corner	TORT			MCNP	TORT
TORT	MCNP	BOC?	location	Total	Thermal	> 27 KeV	> 27 KeV	> 27 KeV
3	G	EOC[a]	3:00	63.6	8.4 [13.2][b]	54.5	47.5 (5)[c]	0.872
			12:00	61.0	6.0 [9.8]	54.4	45.6 (4)	0.838
---	A	EOC	3:00	------	------	------	53.2 (5)	------
			12:00	------	------	------	50.3 (4)	------
7	B	BOC	3:00	59.9	7.0 [11.7]	52.4	44.3 (4)	0.845
			12:00	57.7	5.0 [8.7]	52.2	42.8 (4)	0.820

[a]EOC control position, BOC fuel composition.
[b]Value in brackets is the fraction of the total neutron dpa rate attributed to the thermal neutrons expressed as a percentage.
[c]Value in parentheses is Monte Carlo fractional standard deviation expressed as a percentage.

Table 4. Comparison of dpa rate calculations at the HFIR nozzle corner with the <u>beryllium insert removed</u>

Run ID[a]		EOC/	Nozzle	Neutron dpa rate (x 10^{-12} s^{-1})				MCNP/
			corner	TORT			MCNP	TORT
TORT	MCNP	BOC?	location	Total	Thermal	> 27 KeV	> 27 KeV	> 27 KeV
12	-------	EOC[b]	3:00	79.0	10.0 [12.7][c]	68.2	------	------
			12:00	78.1	7.1 [9.1]	70.1	------	------
8	H	BOC	3:00	74.4	8.3 [11.1]	65.3	58.1 (5)[d]	0.89
			12:00	73.9	5.9 [8.0]	67.3	58.0 (7)	0.86

[a]Number/letter refers to partial name of TORT or MCNP run. See description of models in Appendix C.
[b]EOC control position, BOC fuel composition.
[c]Value in brackets is the fraction of the total neutron dpa rate attributed to the thermal neutrons expressed as a percentage.
[d]Value in parentheses is Monte Carlo fractional standard deviation expressed as a percentage.

3.4 SUMMARY OF RESULTS

Results are summarized as follows:

1. 3-D discrete ordinates (TORT) calculations in which the beryllium insert is approximated as an annulus (Case 4), and thus simulates the earlier 2-D model (Case 1), agree well with the 2-D (DORT) calculations. The 3-D neutron, gamma, and total dpa rates at the nozzle corner were respectively ~7.5 %, ~3%, and ~6% lower than the equivalent 2-D results.

2. Nozzle corner dpa rate calculations in which the actual beryllium insert design (vertical "strips") is modeled are ~20% greater than those in which the annular approximation is used (Table 1 cases 3 and 4). For both the annular and "strip" configurations, the dpa rate is slightly higher at the 3:00 position than at the 12:00 position.

3. For the discrete ordinates calculations, thermal neutrons account for ~12% of the total dpa rate (Table 3), and gammas account for ~6%.

4. A comparison of the discrete ordinates (TORT) and the Monte Carlo (MCNP) calculations (energy > 27 keV) shows that the MCNP dpa rate results are typically ~13% to ~18% lower than the equivalent TORT calculations (Table 3).

5. A comparison of Tables 3 and 4 shows that for a hypothetical case in which the beryllium insert is omitted, the neutron dpa rate at the nozzle corner is increased by ~25%. Thus, the overall effect of the beryllium insert is to shield the nozzle corner a small amount. This difference is consistent for the TORT and the MCNP models and for the total and thermal neutron dpa rate.

3.5 DISCUSSION OF RESULTS

3.5.1 Comparison of dpa rates at nozzle-corner positions 3:00 and 12:00

The longer side of the "rectangular" window in the beryllium insert is oriented vertically, and thus it might be expected that the dpa rate would be higher at the nozzle corner position 12:00 than at 3:00. The opposite result was obtained with both the TORT and MCNP models. It is of interest to note that when the window is circular (cases 4,5,12,E, F, and H), the same result was obtained. This indicates that the non-uniform distribution of the primary source (cylindrical core) near the end of the beam tube is responsible for the somewhat higher dpa rate at nozzle-corner position 3:00 than at 12:00.

3.5.2 Best estimate of dpa rate at nozzle corner

A best estimate of the difference in the HB-2 nozzle corner dpa rates estimated with the 2-D model and the 3-D model that includes the actual beryllium insert design is obtained by comparing the DORT 2-D results (Case 1) with the average of the TORT and MCNP 3-D results. In order to do this, it is necessary to correct the MCNP results because of the low-energy neutron cutoff (27 KeV). Using the position 3:00 data in Table 3 for cases 3 and G, the best-estimate 3-D dpa rate for neutrons is

[63.6 (TORT) + 47.5/0.872 (MCNP corrected)]/2 = 59.0,

which is only 4% higher than the 2-D value (57.0). This small difference indicates that the HB-2 nozzle corner dpa rate used in Reference 3 is only slightly different from the rate derived with a 3-D model

containing the correct beryllium insert. However, all calculated values must be normalized by dosimetry data when applied in the vessel integrity studies, and a new set of dosimetry data is in the offing.[19]

4. REFERENCES

1. R. D. Cheverton, J. G. Merkle, and R. K. Nanstad, *Evaluation of HFIR Pressure Vessel Integrity Considering Radiation Embrittlement*, ORNL/TM-10444, December 1988.

2. R. D. Cheverton, *An Evaluation of Life Extension of the HFIR Pressure Vessel Supplement 1*, ORNL/TM-12877/S1, August 1996.

3. R. D. Cheverton and T. L. Dickson, *HFIR Vessel Life Extension with Enlarged HB-2 and HB-4 Beam Tubes*, ORNL/TM-13698, December 1998.

4. E. D. Blakeman, *Neutron and Gamma Fluxes and dpa Rates for HFIR Vessel Beltline Region (Present and Upgrade Designs)*, ORNL/TM-13693, November 2000.

5. E. D. Blakeman, *Neutron and Gamma Fluxes and dpa Rates for HFIR Vessel Beltline Region (Present and Upgrade Designs) Supplement 1*, ORNL/TM-13693/S1, December 2000.

6. W. A. Rhoades and R. L. Childs, "The DORT Two-Dimensional Discrete Ordinates Transport Code." Nucl. Sci. & Engr. **99**,1,88–89, May 1988.

7. W. A. Rhoades and D. B. Simpson, *The TORT Three-Dimensional Discrete Ordinates Neutron/Photon Transport Code (TORT Version 3)*, ORNL/TM-13221, October 1997.

8. DOORS3.1, RSICC Computer Code Collection, CCC-650, Radiation Safety information Computational Center, Oak Ridge National Laboratory, 1996.

9. C. Y. Fu and D. T. Ingersoll, *VELM61 and VELM22: Multigroup Cross-Section Libraries for Sodium-Cooled Reactor Shield Analysis*, ORNL/TM-10302, April 1987.

10. *1997 Annual Book of ASTM Standards*, Sect. 12, Vol. **12.02**, Nuclear (II), Solar, and Geothermal Energy, 1997.

11. N. P. Baumann, "Gamma-ray Induced Displacements in D2O Reactors," *Proc. of the Seventh ASTM-EURATOM Symposium on Reactor Dosimetry*, Strasbourg, France, August 27–31, 1990.

12. E. D. Blakeman, "P_5 Scattering Order Assessment in HFIR Beam Tube Calculations," Memorandum to J. R. Inger, October 3, 2000.

13. J. F. Briesmeister, Ed, *MCNP – A General Monte Carlo N-Particle Transport Code, Version 4B*, LA-12625-M Vers 4B, Los Alamos National Laboratory, March 1997; code is available from the Radiation Shielding Information Center at ORNL as Code Package CCC-660, April 1997.

14. R. D. Cheverton and T. M. Sims, *HFIR Core Nuclear Design*, ORNL-4621, July 1971.

15. R. T. Primm, III, *Reactor Physics Input to the Safety Analysis Report for the High Flux Isotope Reactor*, ORNL/TM-11956, March 1992.

16. J. A. Bucholz, *Source Terms for HFIR Beam Tube Shielding Analyses, and a Complete Shielding Analysis of the HB-3 Tube*, ORNL/TM-13720, July 2000.

17. J. C. Gehin, Oak Ridge National Laboratory, personal communication to E. D. Blakeman, April 2003.

18. BOLD VENTURE IV, RSICC Computer Code Collection, CCC-459A, Radiation Safety Information Computational Center, Oak Ridge National Laboratory, 1995.

19. R. D. Cheverton, R. K. Nansted, and E. D. Blakeman, *HFIR Pressure Vessel and Structural Components Materials Surveillance Program, Supplement 2*, ORNL/TM-1372/S2, August 1999.

APPENDIX A

VELM61 CROSS-SECTION SET AND GROUP STRUCTURE

The VELM61 broad-group cross-section library, which is collapsed from the fine-group, 212-group Vitamin-E library, contains 61 neutron groups and 23 gamma groups. The neutron group structure contains one thermal neutron group; thus, neutron energy upscattering is not treated. Tables A.1 and A.2 show the neutron and gamma group boundaries as well as the iron dpa cross-sections. From Table A.1 it is observed that the neutron dpa cross section decreases monotonically with energy from ~15 MeV to about 100 eV, below which it begins to increase slightly. From Table A.2, the gamma dpa cross-section decreases monotonically from ~14 MeV to about 1 MeV, below which it is negligible.

Table A.1 VELM61 neutron group boundaries and iron dpa cross sections

Group	Upper energy (eV)	Iron dpa (cm^2)	Group	Upper energy (eV)	Iron dpa (cm^2)
1	1.4918e+7	2.744e-21	31	1.2277e+5	1.075e-22
2	1.2214e+7	2.446e-21	32	8.6517e+4	1.100e-22
3	1.0000e+7	2.213e-21	33	5.6562e+4	7.913e-23
4	8.1873e+6	2.037e-21	34	5.2475e+4	6.693e-23
5	6.7032e+6	1.874e-21	35	3.4307e+4	2.042e-22
6	5.4881e+6	1.718e-21	36	2.8501e+4	4.334e-22
7	4.4933e+6	1.539e-21	37	2.7000e+4	6.080e-23
8	3.6788e+6	1.371e-21	38	2.6058e+4	2.889e-23
9	3.0119e+6	1.272e-21	39	2.4788e+4	3.810e-24
10	2.4660e+6	1.161e-21	40	2.3579e+4	7.355e-24
11	2.3457e+6	1.042e-21	41	1.5034e+4	1.194e-23
12	2.2313e+6	1.047e-21	42	9.1188e+3	2.400e-23
13	2.0190e+6	8.667e-22	43	5.5308e+3	6.707e-24
14	1.6530e+6	8.127e-22	44	3.7074e+3	4.857e-24
15	1.3534e+6	5.900e-22	45	3.0354e+3	4.156e-24
16	1.1080e+6	4.302e-22	46	2.6126e+3	3.666e-24
17	9.0718e+5	4.658e-22	47	2.2487e+3	3.245e-24
18	7.4274e+5	3.612e-22	48	2.0347e+3	2.426e-24
19	6.0810e+5	2.747e-22	49	1.2341e+3	3.410e-24
20	5.2340e+5	3.605e-22	50	7.4852e+2	2.234e-25
21	4.9787e+5	3.946e-22	51	4.5400e+2	9.134e-26
22	3.8774e+5	2.480e-22	52	2.7536e+2	1.173e-25
23	3.0197e+5	1.638e-22	53	1.6702e+2	1.506e-25
24	2.9849e+5	1.921e-22	54	1.0130e+2	2.038e-25
25	2.9721e+5	1.921e-22	55	4.7851e+1	2.966e-25
26	2.9452e+5	2.077e-22	56	2.2603e+1	4.315e-25
27	2.7324e+5	1.754e-22	57	1.0677e+1	6.278e-25
28	2.2371e+5	2.196e-22	58	5.0435e+0	9.135e-25
29	1.8316e+5	1.399e-22	59	2.3824e+0	1.326e-24
30	1.4996e+5	1.781e-22	60	1.1253e+0	2.031e-24
			61	4.1399e-1	5.296e-24

Table A.2 VELM61 gamma group boundaries and iron dpa cross sections

Group	Upper energy (eV)	Iron dpa (cm^2)	Group	Upper energy (eV)	Iron dpa (cm^2)
1	1.4e+7	7.600e-24	13	1.0e+6	4.333e-27
2	1.0e+7	6.249e-24	14	7.0e+5	0
3	8.0e+6	4.677e-24	15	6.0e+5	0
4	7.5e+6	4.111e-24	16	5.1e+5	0
5	7.0e+6	3.314e-24	17	4.0e+5	0
6	6.0e+6	2.388e-24	18	3.0e+5	0
7	5.0e+6	1.585e-24	19	1.5e+5	0
8	4.0e+6	9.269e-25	20	1.0e+5	0
9	3.0e+6	5.278e-25	21	7.0e+4	0
10	2.5e+6	3.133e-25	22	4.5e+4	0
11	2.0e+6	1.456e-25	23	2.0e+4	0
12	1.5e+6	4.030e-26			

APPENDIX B

160-ANGLE X-AXIS STREAMING QUADRATURE

Weights and direction cosines for the 160-direction TORT-based quadrature are listed in Table B.1. The quadrature is designed for particle streaming along the X-axis.

Table B.1. 160-angle X-axis streaming quadrature

X, Y, Z - axis direction cosines

	Weight	X	Y	Z
1	0.00000E+00	-9.80000E-01	0.00000E+00	-1.99000E-01
2	1.15005E-02	-9.62250E-01	-1.92452E-01	-1.92450E-01
3	8.73399E-03	-8.38870E-01	-5.09176E-01	-1.92450E-01
4	8.73399E-03	-8.38870E-01	-1.92439E-01	-5.09180E-01
5	6.17300E-03	-6.93890E-01	-6.93887E-01	-1.92450E-01
6	6.52549E-03	-6.93890E-01	-5.09168E-01	-5.09180E-01
7	6.17300E-03	-6.93890E-01	-1.92441E-01	-6.93890E-01
8	8.73399E-03	-5.09180E-01	-8.38867E-01	-1.92450E-01
9	6.52549E-03	-5.09180E-01	-6.93881E-01	-5.09180E-01
10	6.52549E-03	-5.09180E-01	-5.09168E-01	-6.93890E-01
11	8.73399E-03	-5.09180E-01	-1.92439E-01	-8.38870E-01
12	1.15005E-02	-1.92450E-01	-9.62250E-01	-1.92450E-01
13	8.73399E-03	-1.92450E-01	-8.38867E-01	-5.09180E-01
14	6.17300E-03	-1.92450E-01	-6.93887E-01	-6.93890E-01
15	8.73399E-03	-1.92450E-01	-5.09176E-01	-8.38870E-01
16	1.15005E-02	-1.92450E-01	-1.92452E-01	-9.62250E-01
17	8.73399E-03	8.38870E-01	-5.09176E-01	-1.92450E-01
18	8.73399E-03	8.38870E-01	-1.92439E-01	-5.09180E-01
19	6.17300E-03	6.93890E-01	-6.93887E-01	-1.92450E-01
20	6.52549E-03	6.93890E-01	-5.09168E-01	-5.09180E-01
21	6.17300E-03	6.93890E-01	-1.92441E-01	-6.93890E-01
22	8.73399E-03	5.09180E-01	-8.38867E-01	-1.92450E-01
23	6.52549E-03	5.09180E-01	-6.93881E-01	-5.09180E-01
24	6.52549E-03	5.09180E-01	-5.09168E-01	-6.93890E-01
25	8.73399E-03	5.09180E-01	-1.92439E-01	-8.38870E-01
26	1.15005E-02	1.92450E-01	-9.62250E-01	-1.92450E-01
27	8.73399E-03	1.92450E-01	-8.38867E-01	-5.09180E-01
28	6.17300E-03	1.92450E-01	-6.93887E-01	-6.93890E-01
29	8.73399E-03	1.92450E-01	-5.09176E-01	-8.38870E-01
30	1.15005E-02	1.92450E-01	-1.92452E-01	-9.62250E-01
31	6.20351E-04	9.97519E-01	-4.97827E-02	-4.97828E-02
32	9.03532E-04	9.87809E-01	-5.95746E-02	-1.43821E-01
33	9.03532E-04	9.87809E-01	-1.43822E-01	-5.95728E-02
34	9.48100E-04	9.69204E-01	-6.37364E-02	-2.37870E-01
35	9.48100E-04	9.69204E-01	-1.74133E-01	-1.74133E-01
36	9.48100E-04	9.69204E-01	-2.37870E-01	-6.37371E-02
37	1.55720E-03	9.32911E-01	-7.02554E-02	-3.53187E-01
38	1.55720E-03	9.32911E-01	-2.00065E-01	-2.99418E-01
39	1.55720E-03	9.32911E-01	-2.99418E-01	-2.00064E-01
40	1.55720E-03	9.32911E-01	-3.53187E-01	-7.02533E-02
41	0.00000E+00	-9.80000E-01	0.00000E+00	-1.99000E-01
42	1.15005E-02	-9.62250E-01	1.92452E-01	-1.92450E-01

Table B.1, cont.

	Weight	X	Y	Z
43	8.73399E-03	-8.38870E-01	5.09176E-01	-1.92450E-01
44	8.73399E-03	-8.38870E-01	1.92439E-01	-5.09180E-01
45	6.17300E-03	-6.93890E-01	6.93887E-01	-1.92450E-01
46	6.52549E-03	-6.93890E-01	5.09168E-01	-5.09180E-01
47	6.17300E-03	-6.93890E-01	1.92441E-01	-6.93890E-01
48	8.73399E-03	-5.09180E-01	8.38867E-01	-1.92450E-01
49	6.52549E-03	-5.09180E-01	6.93881E-01	-5.09180E-01
50	6.52549E-03	-5.09180E-01	5.09168E-01	-6.93890E-01
51	8.73399E-03	-5.09180E-01	1.92439E-01	-8.38870E-01
52	1.15005E-02	-1.92450E-01	9.62250E-01	-1.92450E-01
53	8.73399E-03	-1.92450E-01	8.38867E-01	-5.09180E-01
54	6.17300E-03	-1.92450E-01	6.93887E-01	-6.93890E-01
55	8.73399E-03	-1.92450E-01	5.09176E-01	-8.38870E-01
56	1.15005E-02	-1.92450E-01	1.92452E-01	-9.62250E-01
57	8.73399E-03	8.38870E-01	5.09176E-01	-1.92450E-01
58	8.73399E-03	8.38870E-01	1.92439E-01	-5.09180E-01
59	6.17300E-03	6.93890E-01	6.93887E-01	-1.92450E-01
60	6.52549E-03	6.93890E-01	5.09168E-01	-5.09180E-01
61	6.17300E-03	6.93890E-01	1.92441E-01	-6.93890E-01
62	8.73399E-03	5.09180E-01	8.38867E-01	-1.92450E-01
63	6.52549E-03	5.09180E-01	6.93881E-01	-5.09180E-01
64	6.52549E-03	5.09180E-01	5.09168E-01	-6.93890E-01
65	8.73399E-03	5.09180E-01	1.92439E-01	-8.38870E-01
66	1.15005E-02	1.92450E-01	9.62250E-01	-1.92450E-01
67	8.73399E-03	1.92450E-01	8.38867E-01	-5.09180E-01
68	6.17300E-03	1.92450E-01	6.93887E-01	-6.93890E-01
69	8.73399E-03	1.92450E-01	5.09176E-01	-8.38870E-01
70	1.15005E-02	1.92450E-01	1.92452E-01	-9.62250E-01
71	6.20351E-04	9.97519E-01	4.97827E-02	-4.97828E-02
72	9.03532E-04	9.87809E-01	5.95746E-02	-1.43821E-01
73	9.03532E-04	9.87809E-01	1.43822E-01	-5.95728E-02
74	9.48100E-04	9.69204E-01	6.37364E-02	-2.37870E-01
75	9.48100E-04	9.69204E-01	1.74133E-01	-1.74133E-01
76	9.48100E-04	9.69204E-01	2.37870E-01	-6.37371E-02
77	1.55720E-03	9.32911E-01	7.02554E-02	-3.53187E-01
78	1.55720E-03	9.32911E-01	2.00065E-01	-2.99418E-01
79	1.55720E-03	9.32911E-01	2.99418E-01	-2.00064E-01
80	1.55720E-03	9.32911E-01	3.53187E-01	-7.02533E-02
81	0.00000E+00	-9.80000E-01	0.00000E+00	1.99000E-01
82	1.15005E-02	-9.62250E-01	-1.92452E-01	1.92450E-01
83	8.73399E-03	-8.38870E-01	-5.09176E-01	1.92450E-01
84	8.73399E-03	-8.38870E-01	-1.92439E-01	5.09180E-01
85	6.17300E-03	-6.93890E-01	-6.93887E-01	1.92450E-01
86	6.52549E-03	-6.93890E-01	-5.09168E-01	5.09180E-01
87	6.17300E-03	-6.93890E-01	-1.92441E-01	6.93890E-01
88	8.73399E-03	-5.09180E-01	-8.38867E-01	1.92450E-01
89	6.52549E-03	-5.09180E-01	-6.93881E-01	5.09180E-01
90	6.52549E-03	-5.09180E-01	-5.09168E-01	6.93890E-01
91	8.73399E-03	-5.09180E-01	-1.92439E-01	8.38870E-01
92	1.15005E-02	-1.92450E-01	-9.62250E-01	1.92450E-01
93	8.73399E-03	-1.92450E-01	-8.38867E-01	5.09180E-01
94	6.17300E-03	-1.92450E-01	-6.93887E-01	6.93890E-01
95	8.73399E-03	-1.92450E-01	-5.09176E-01	8.38870E-01

Table B.1, cont.

	Weight	X	Y	Z
96	1.15005E-02	-1.92450E-01	-1.92452E-01	9.62250E-01
97	8.73399E-03	8.38870E-01	-5.09176E-01	1.92450E-01
98	8.73399E-03	8.38870E-01	-1.92439E-01	5.09180E-01
99	6.17300E-03	6.93890E-01	-6.93887E-01	1.92450E-01
100	6.52549E-03	6.93890E-01	-5.09168E-01	5.09180E-01
101	6.17300E-03	6.93890E-01	-1.92441E-01	6.93890E-01
102	8.73399E-03	5.09180E-01	-8.38867E-01	1.92450E-01
103	6.52549E-03	5.09180E-01	-6.93881E-01	5.09180E-01
104	6.52549E-03	5.09180E-01	-5.09168E-01	6.93890E-01
105	8.73399E-03	5.09180E-01	-1.92439E-01	8.38870E-01
106	1.15005E-02	1.92450E-01	-9.62250E-01	1.92450E-01
107	8.73399E-03	1.92450E-01	-8.38867E-01	5.09180E-01
108	6.17300E-03	1.92450E-01	-6.93887E-01	6.93890E-01
109	8.73399E-03	1.92450E-01	-5.09176E-01	8.38870E-01
110	1.15005E-02	1.92450E-01	-1.92452E-01	9.62250E-01
111	6.20351E-04	9.97519E-01	-4.97827E-02	4.97828E-02
112	9.03532E-04	9.87809E-01	-5.95746E-02	1.43821E-01
113	9.03532E-04	9.87809E-01	-1.43822E-01	5.95728E-02
114	9.48100E-04	9.69204E-01	-6.37364E-02	2.37870E-01
115	9.48100E-04	9.69204E-01	-1.74133E-01	1.74133E-01
116	9.48100E-04	9.69204E-01	-2.37870E-01	6.37371E-02
117	1.55720E-03	9.32911E-01	-7.02554E-02	3.53187E-01
118	1.55720E-03	9.32911E-01	-2.00065E-01	2.99418E-01
119	1.55720E-03	9.32911E-01	-2.99418E-01	2.00064E-01
120	1.55720E-03	9.32911E-01	-3.53187E-01	7.02533E-02
121	0.00000E+00	-9.80000E-01	0.00000E+00	1.99000E-01
122	1.15005E-02	-9.62250E-01	1.92452E-01	1.92450E-01
123	8.73399E-03	-8.38870E-01	5.09176E-01	1.92450E-01
124	8.73399E-03	-8.38870E-01	1.92439E-01	5.09180E-01
125	6.17300E-03	-6.93890E-01	6.93887E-01	1.92450E-01
126	6.52549E-03	-6.93890E-01	5.09168E-01	5.09180E-01
127	6.17300E-03	-6.93890E-01	1.92441E-01	6.93890E-01
128	8.73399E-03	-5.09180E-01	8.38867E-01	1.92450E-01
129	6.52549E-03	-5.09180E-01	6.93881E-01	5.09180E-01
130	6.52549E-03	-5.09180E-01	5.09168E-01	6.93890E-01
131	8.73399E-03	-5.09180E-01	1.92439E-01	8.38870E-01
132	1.15005E-02	-1.92450E-01	9.62250E-01	1.92450E-01
133	8.73399E-03	-1.92450E-01	8.38867E-01	5.09180E-01
134	6.17300E-03	-1.92450E-01	6.93887E-01	6.93890E-01
135	8.73399E-03	-1.92450E-01	5.09176E-01	8.38870E-01
136	1.15005E-02	-1.92450E-01	1.92452E-01	9.62250E-01
137	8.73399E-03	8.38870E-01	5.09176E-01	1.92450E-01
138	8.73399E-03	8.38870E-01	1.92439E-01	5.09180E-01
139	6.17300E-03	6.93890E-01	6.93887E-01	1.92450E-01
140	6.52549E-03	6.93890E-01	5.09168E-01	5.09180E-01
141	6.17300E-03	6.93890E-01	1.92441E-01	6.93890E-01
142	8.73399E-03	5.09180E-01	8.38867E-01	1.92450E-01
143	6.52549E-03	5.09180E-01	6.93881E-01	5.09180E-01
144	6.52549E-03	5.09180E-01	5.09168E-01	6.93890E-01
145	8.73399E-03	5.09180E-01	1.92439E-01	8.38870E-01
146	1.15005E-02	1.92450E-01	9.62250E-01	1.92450E-01
147	8.73399E-03	1.92450E-01	8.38867E-01	5.09180E-01
148	6.17300E-03	1.92450E-01	6.93887E-01	6.93890E-01

Table B.1, cont.

	Weight	X	Y	Z
149	8.73399E-03	1.92450E-01	5.09176E-01	8.38870E-01
150	1.15005E-02	1.92450E-01	1.92452E-01	9.62250E-01
151	6.20351E-04	9.97519E-01	4.97827E-02	4.97828E-02
152	9.03532E-04	9.87809E-01	5.95746E-02	1.43821E-01
153	9.03532E-04	9.87809E-01	1.43822E-01	5.95728E-02
154	9.48100E-04	9.69204E-01	6.37364E-02	2.37870E-01
155	9.48100E-04	9.69204E-01	1.74133E-01	1.74133E-01
156	9.48100E-04	9.69204E-01	2.37870E-01	6.37371E-02
157	1.55720E-03	9.32911E-01	7.02554E-02	3.53187E-01
158	1.55720E-03	9.32911E-01	2.00065E-01	2.99418E-01
159	1.55720E-03	9.32911E-01	2.99418E-01	2.00064E-01
160	1.55720E-03	9.32911E-01	3.53187E-01	7.02533E-02

APPENDIX C

MODEL SUMMARY AND DATA ARCHIVE

This appendix summarizes configuration model names and addresses the archive of computer input/output files. Archived information has been provided to HFIR.

Table C.1 describes equivalent TORT and MCNP runs for discrete ordinates and Monte Carlo model configurations.

Table C1. Equivalent TORT and MCNP runs for discrete ordinates and Monte Carlo model configurations

Configuration Description		Input files	
Beryllium Insert	**BOC/EOC Fuel & Control**	**TORT[a]**	**MCNP[b]**
Strips	EOC	--------	A
	EOC[c]	3	G
	BOC	7	B
Annulus	EOC	--------	E
	EOC[c]	4	------
	BOC	11	F
None	EOC[c]	12	------
	BOC	8	H

[a]Complete name of file is "tort.hb2.upgrade.*.sh" where "*" refers to run number given in column; e.g., "3" is equivalent to "tort.hb2.upgrade.3.sh".
[b]Complete name of file is "hf245*a", where * refers to the letter given in the column; e.g., "A" is equivalent to "hf245Aa". The final letter "a" is the preliminary run for 1×10^6 histories. Runs with the final letter "b" have 5×10^6 histories. Runs with a greater number of histories have sequential letters (i.e., "c", "d", etc.) at the end, where each subsequent letter represents a doubling of the number of histories; e.g., hf245Ae would be the input for 40×10^6 histories. However, for most cases above 10×10^6 histories, an additional input file was not written other than a brief "restart" file with only a few lines that contains the increased number of histories required. Thus, file names ending in "a" serve as basic input.
[c]Control positions are EOC, but fuel is BOC configuration.

The Monte Carlo MCNP model includes the entire HFIR reactor and beam tubes. However, the discrete ordinates TORT model only includes a portion of the core and vessel containing the HB-2 beam tube. Source inputs are generated by an additional model of the reactor and auxiliary codes to write the source in the proper format. Table C.2 lists the additional files required. The codes are also arranged in sequence.

Table C.2. Auxiliary code sequence for discrete ordinates TORT runs

Code	Description/purpose	File name	Comments
DORT	2-D model of reactor core Calculates fuel fission density	hfr84k.sh11 hfr84k.sh21	EOC control. 2nd file (sh21) outputs fission densities
		hfr84k.boc.sh11 hfr84k.boc.sh21	BOC control. 2nd file (sh21) outputs fission densities
DORT	2-D model of reactor core & vessel Calculates neutron and gamma scalar and directional fluxes	hfr84fs.extendedR.s16.sh	EOC control
		hfr84fs.dg.extendedR.s16.sh	Same as above for delayed gamma source
		hfr84fs.extendedR.boc.s16.sh	BOC
		hfr84fs.dg.extendedR.boc.s16.sh	Same as above but for delayed gamma source
VISA	Auxiliary code that reorders and reformats directional flux for TORSED input	hfr84vis.hb2.tort.s16.sh	EOC control
		hfr84vis.dg.hb2.tort.s16.sh	Same as above for delayed gamma source
		hfr84vis.hb2.tort.boc.s16.sh	BOC
TORSED	Auxiliary code that writes source boundary file for TORT model	Torsed.hb2.upgrade.*.sh	"*" corresponds to TORT model run number

Table C.3 further summarizes information relating to the computer hardware and software used to perform the discrete ordinates and Monte Carlo analyses. This information provides a vital "snapshot" of systems used such that results could be duplicated exactly if required. It is noted that the code systems employed for these calculations are widely used in the nuclear industry and undergo a rigorous qualification process. As a result, the codes give exact or equivalent results for a broad range of computers and compilers. New releases of codes give either equivalent or improved results compared with earlier releases.

Table C.3. Computer hardware/software used for discrete ordinates and Monte Carlo analyses

Computer/model information	**Transport model type**	
	discrete ordinates	**Monte Carlo**
Computer system name	NAS7	CPILE
Computer type/model	IBM/RS6000 Model 43P	KC-Computer Co., "IBM" compatible
Operating system/version	AIX 4.3	Red Hat Linux 7.3
Computer code/version	DOORS 3.3	MCNP Ver. 4C
Type of compiler	XL FORTRAN for AIX Ver. 08.01.0000.0002	LINUX Portland Group FORTRAN 4.0.2
Owner of code	ORNL (DOORS)	LANL (MCNP)
RSICC[a] distribution number	CCC65/DOORS3.2[b]	CCC700/MCNP4

[a]Radiation Safety Information Computational Center (RSICC) located and operated within the Nuclear Science and Technology Division at ORNL.

[b]Calculations were performed with DOORS3.3, which is a revised version of the DOORS3.2 system, but available on a limited basis. A subset of the calculations was also performed using DOORS3.2 which is openly distributed by RSICC. Numerical differences between the DOORS3.2 and DOORS3.3 calculations were insignificant.

APPENDIX D

FUEL REGION U-235 ATOM DENSITIES AND ZONE BOUNDARIES FOR DISCRETE ORDINATES AND MONTE CARLO CALCULATION MODELS

Figure D.1 shows a diagram of the fuel zones used in the discrete ordinates calculations and is obtained from models used in a 1992 diffusion theory 3-D analysis[1] of the HFIR core. The inner and outer fuel annuli in this approach are together divided into 14 "effective" zones. There are in fact 18 zones in the model, but four are only 0.01-cm-thick and are in the model primarily for examining edge effects. Boundaries for the 17 fuel zones (actually "cell" boundaries) in the Monte Carlo model were obtained from an earlier analysis[2] and are shown superimposed on the discrete ordinates boundaries. Figures D.2 and D.3 show U^{235} atom densities for the inner and outer fuel annuli for the two models, respectively. It is evident that with regard to the U^{235} content, the models are essentially interpolations of each other and are approximately equivalent. Similar equivalencies also exist for the other material constituents.

References for Appendix D

1. R. T. Primm, III, *Reactor Physics Input to the Safety Analysis Report for the High Flux Isotope Reactor*, ORNL/TM-11956, March 1992.

2. R. D. Cheverton and T. M. Sims, *HFIR Core Nuclear Design*, ORNL-4621, July 1971.

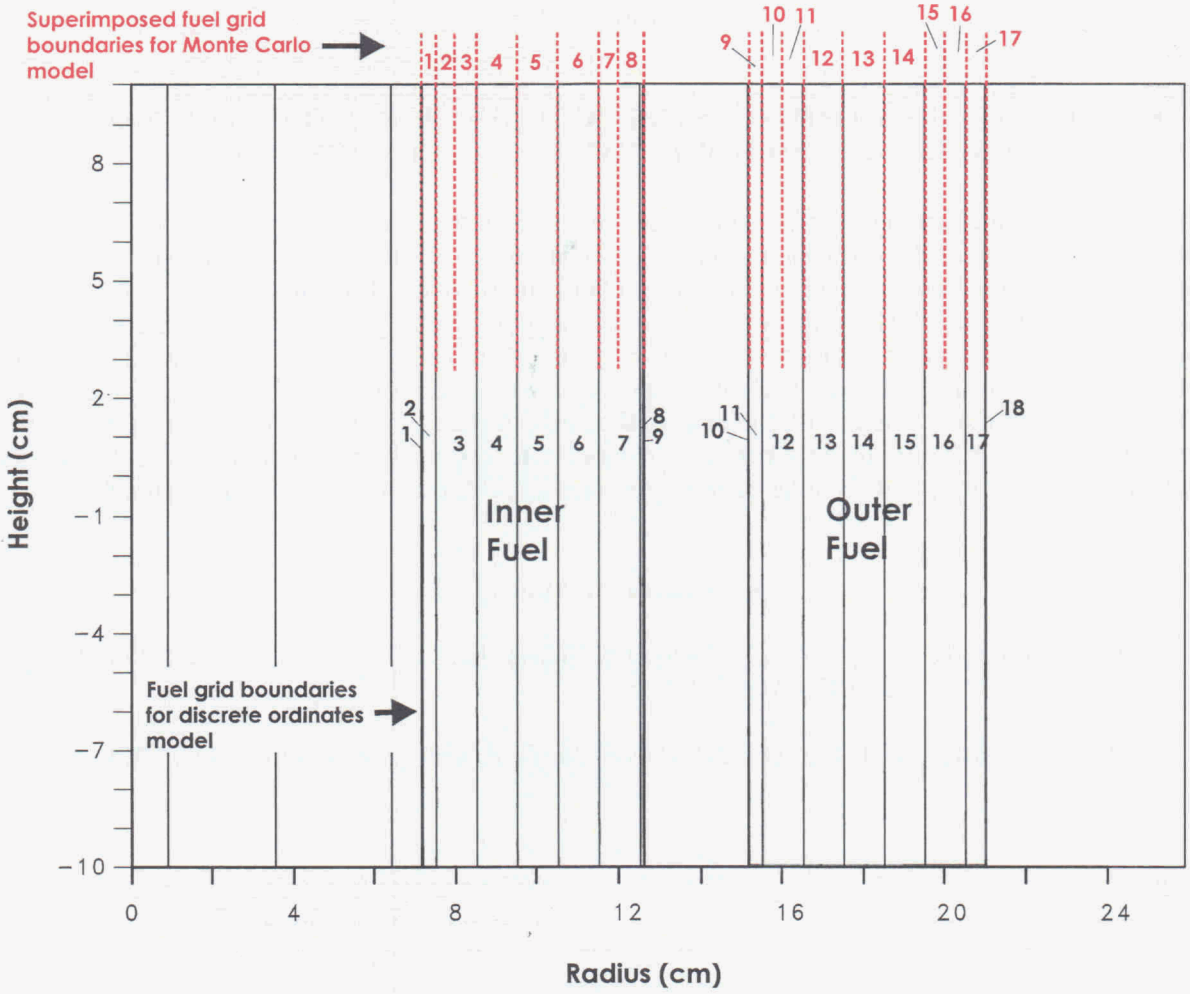

Figure D.1 Schematic of HFIR fueled region boundaries for 2-D discrete ordinates model showing superimposed Monte Carlo cell boundaries.

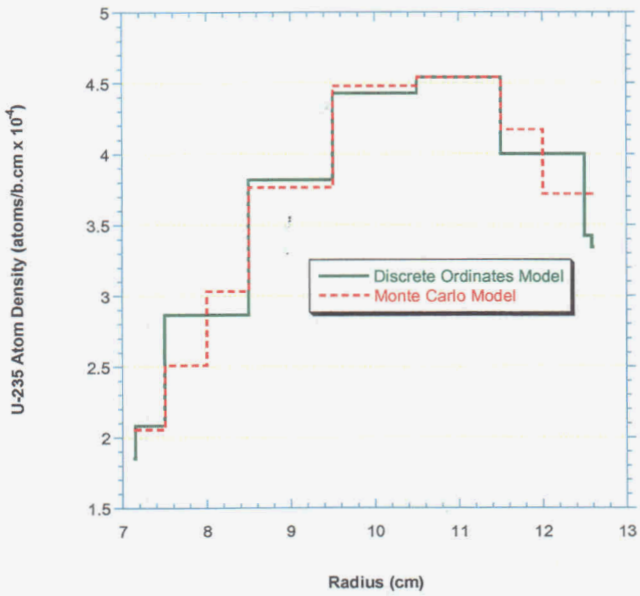

Figure D.2 Plot of U^{235} atom density for discrete ordinates and Monte Carlo models vs radius for the HFIR <u>inner</u> fuel annulus.

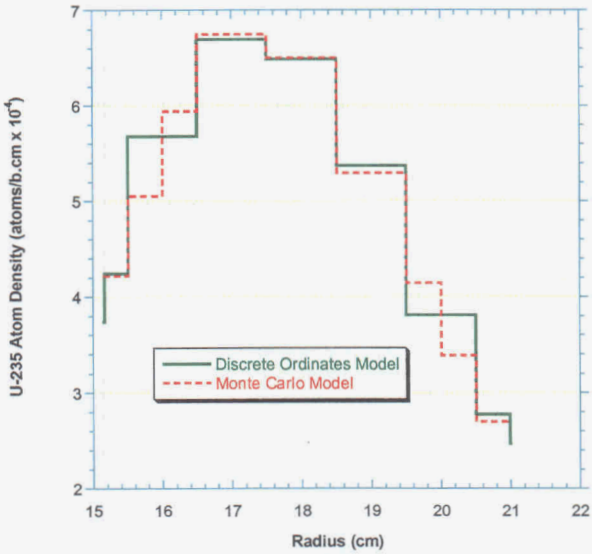

Figure D.3 Plot of U^{235} atom density for discrete ordinates and Monte Carlo models vs radius for the HFIR <u>outer</u> fuel annulus.

APPENDIX E

ISO-PLOTS OF DPA RATE CALCULATIONS

Plots for the following dpa rate calculations listed in Table E.1 are shown in Figures E.1 – E.20

Table E.1 Listing of iso-plots for TORT dpa rate calculations

TORT ID	EOC/ BOC?	Beryllium insert configuration[a]	Plot orientation[b]	dpa rate plot type	Plot figure number
7	BOC	Strips	Plan	Neutron	E.1
			Elevation	Neutron	E.2
			Plan	Gamma	E.3
			Elevation	Gamma	E.4
4	EOC[c]	Annulus	Plan	Neutron	E.5
			Elevation	Neutron	E.6
			Plan	Gamma	E.7
			Elevation	Gamma	E.8
11	BOC	Annulus	Plan	Neutron	E.9
			Elevation	Neutron	E.10
			Plan	Gamma	E.11
			Elevation	Gamma	E.12
12	EOC[c]	No insert	Plan	Neutron	E.13
			Elevation	Neutron	E.14
			Plan	Gamma	E.15
			Elevation	Gamma	E.16
8	BOC	No insert	Plan	Neutron	E.17
			Elevation	Neutron	E.18
			Plan	Gamma	E.19
			Elevation	Gamma	E.20

[a] "Strips" refers to the as-designed insert as two vertical strips that line the inside of the beam tube. "Annulus" refers to a simplified annular insert that simulates the 2-D approach. Runs performed with no insert were intended to determine the overall effect of the insert.
[b] "Plan" orientation is a horizontal plane located at the vertical mid-plane of the reactor. "Elevation" orientation is a vertical plane parallel to the beam tube and bisecting it along the beam tube axis.
[c] Control is in EOC configuration; fuel is in BOC configuration.

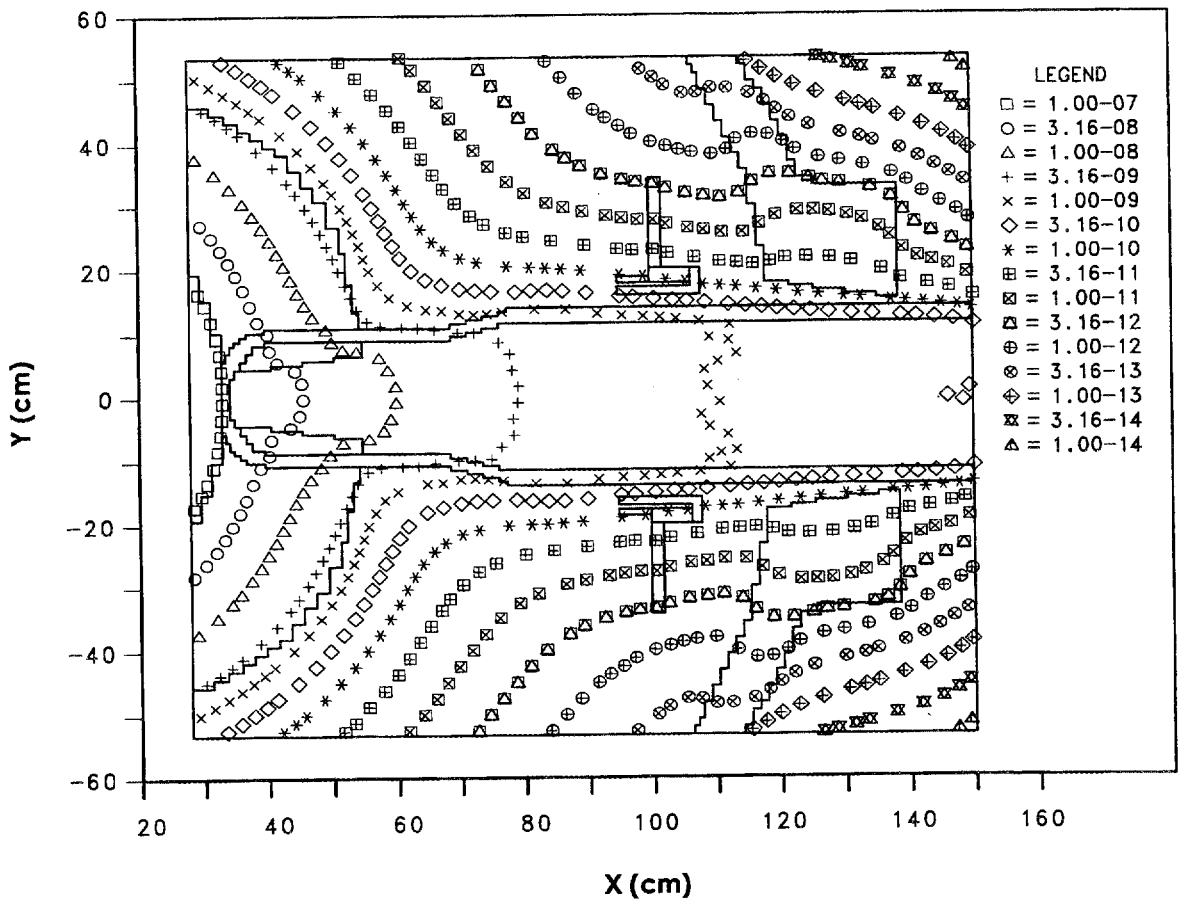

Figure E.1. Iso-plot of neutron dpa rate for HFIR HB-2 modified design for BOC conditions; plan view — horizontal cut along beam tube axis.

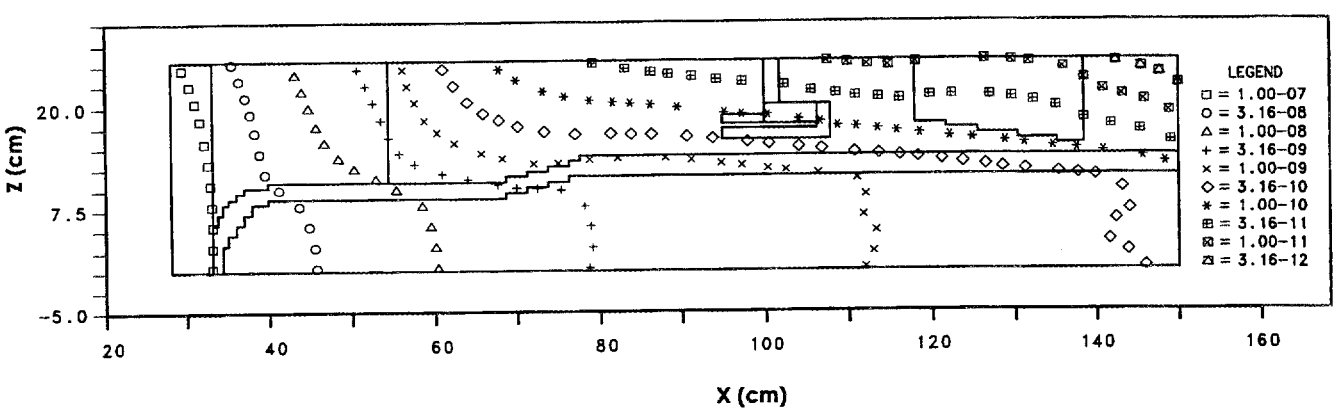

Figure E.2. Iso-plot of neutron dpa rate for HFIR HB-2 modified design for BOC conditions; elevation view — vertical cut along beam tube axis.

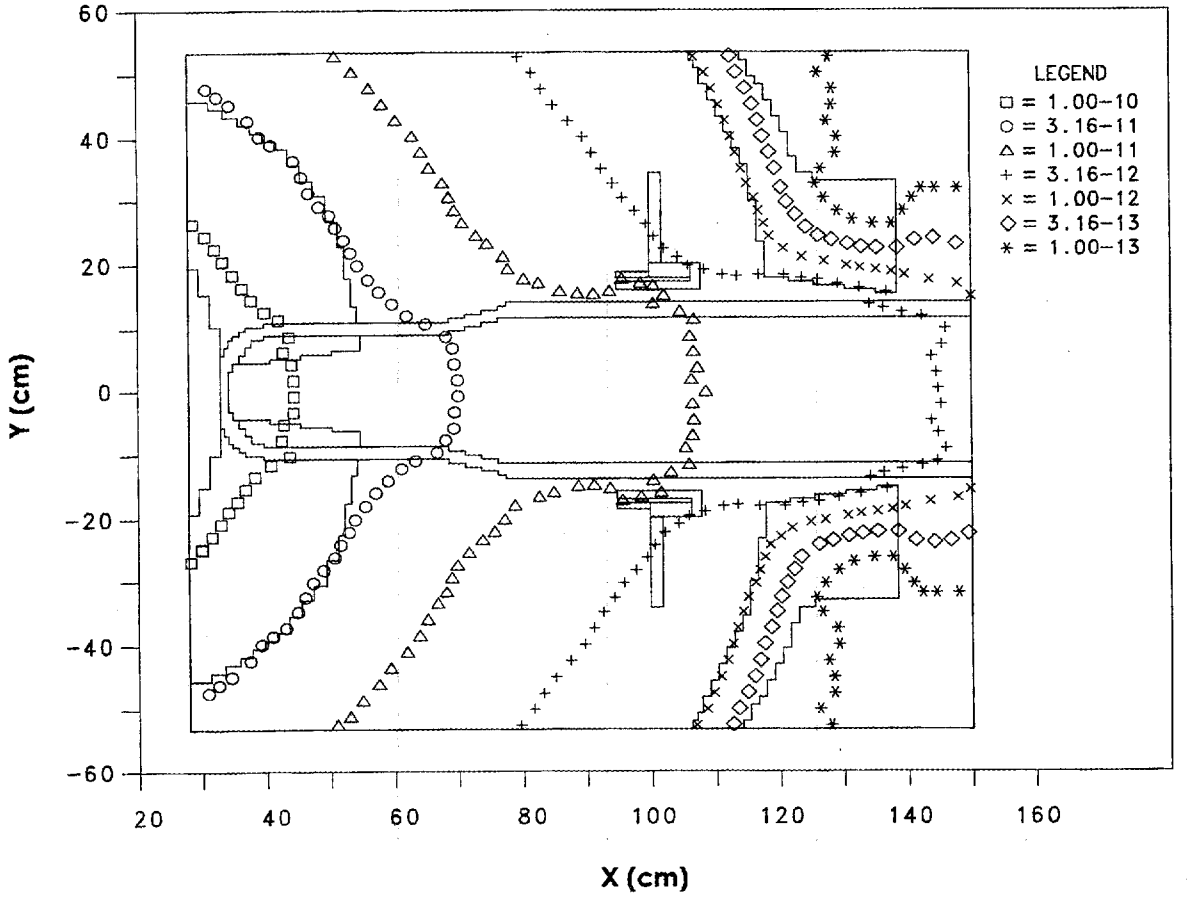

Figure E.3. Iso-plot of gamma dpa rate for HFIR HB-2 modified design for BOC conditions; plan view — horizontal cut along beam tube axis.

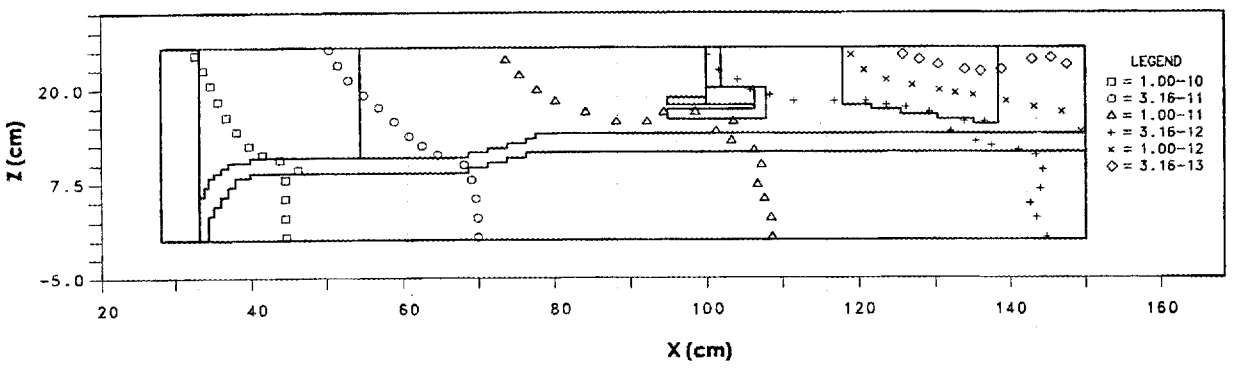

Figure E.4. Iso-plot of gamma dpa rate for HFIR HB-2 modified design for BOC conditions; elevation view — vertical cut along beam tube axis.

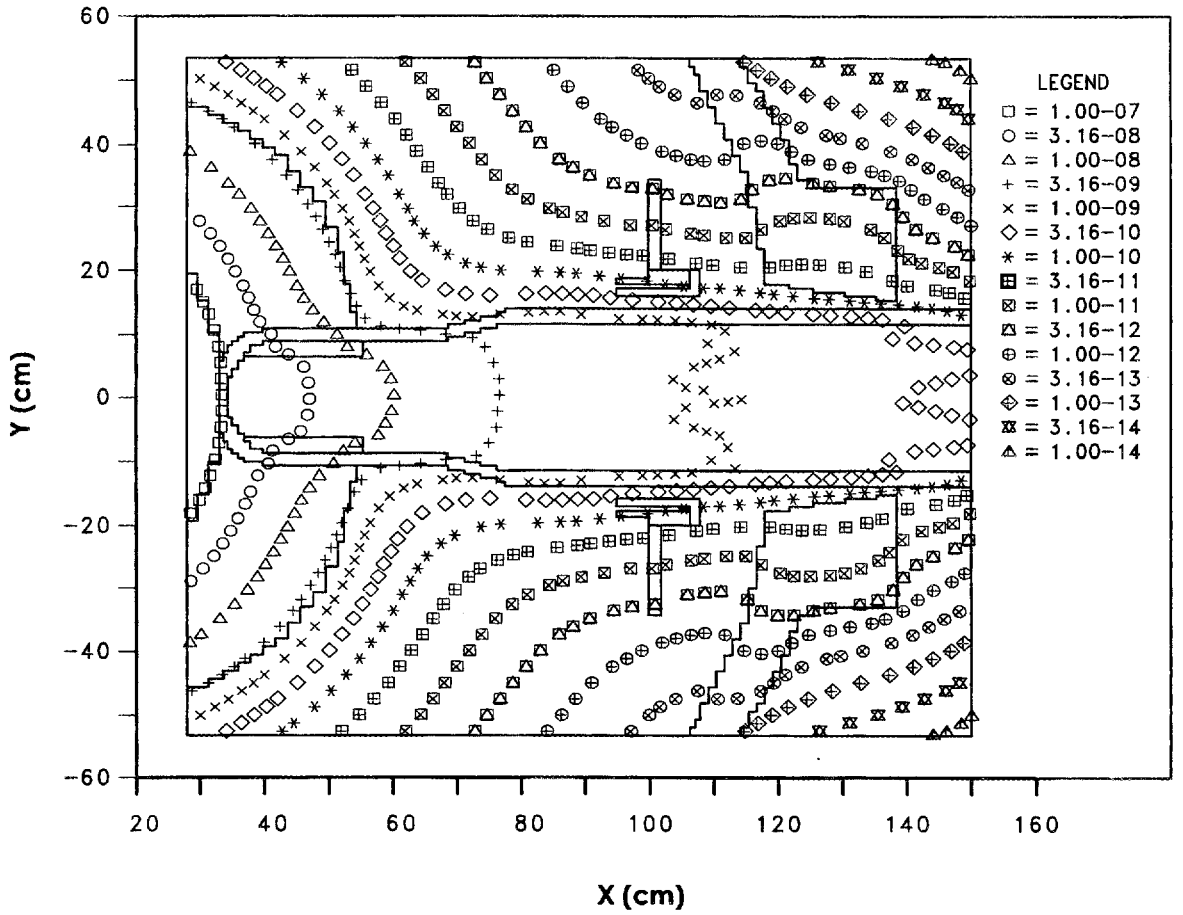

Figure E.5. Iso-plot of neutron dpa rate for HFIR HB-2 modified design for EOC conditions; annular beryllium insert; plan view — horizontal cut along beam tube axis.

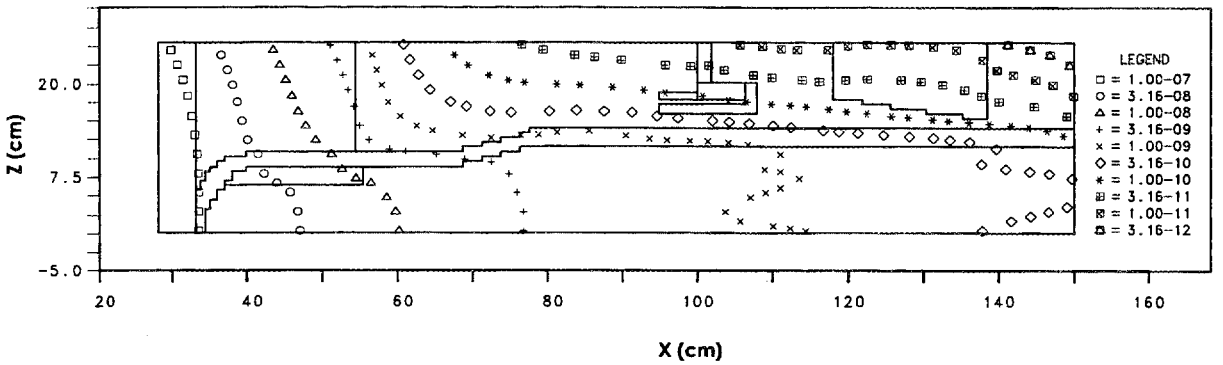

Figure E.6. Iso-plot of neutron dpa rate for HFIR HB-2 modified design for EOC conditions; annular beryllium insert; elevation view — vertical cut along beam tube axis.

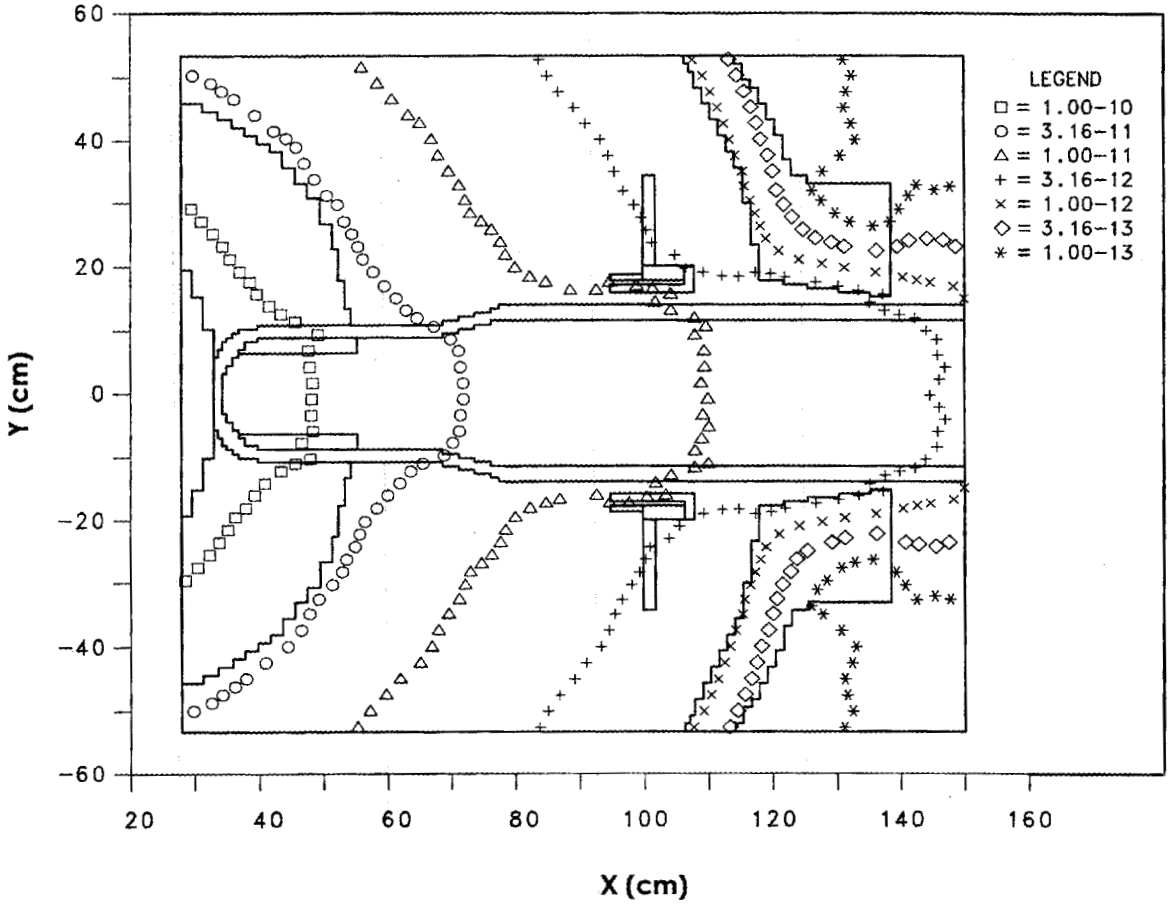

Figure E.7. Iso-plot of gamma dpa rate for HFIR HB-2 modified design for EOC conditions; annular beryllium insert; plan view — horizontal cut along beam tube axis.

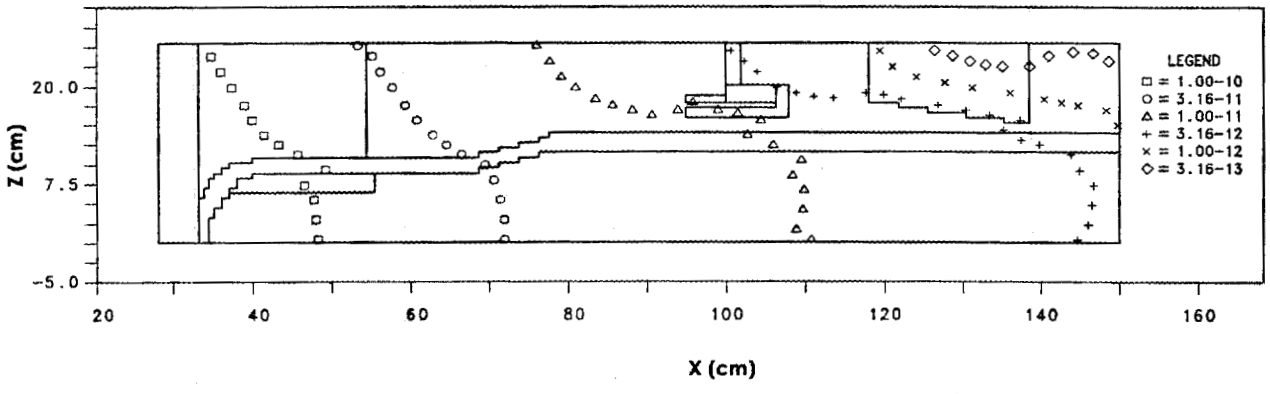

Figure E.8. Iso-plot of gamma dpa rate for HFIR HB-2 modified design for EOC conditions; annular beryllium insert; elevation view — vertical cut along beam tube axis.

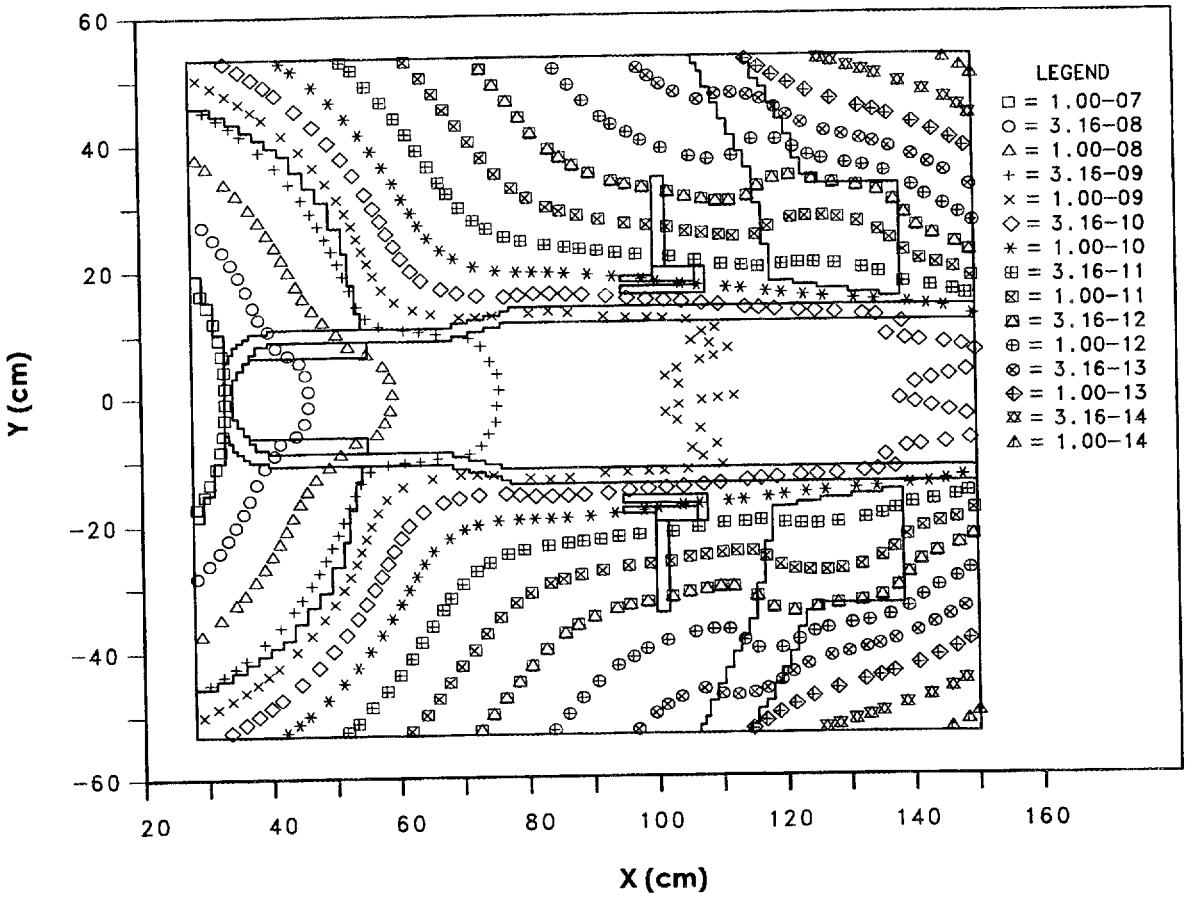

Figure E.9. Iso-plot of neutron dpa rate for HFIR HB-2 modified design for BOC conditions; annular beryllium insert; plan view — horizontal cut along beam tube axis.

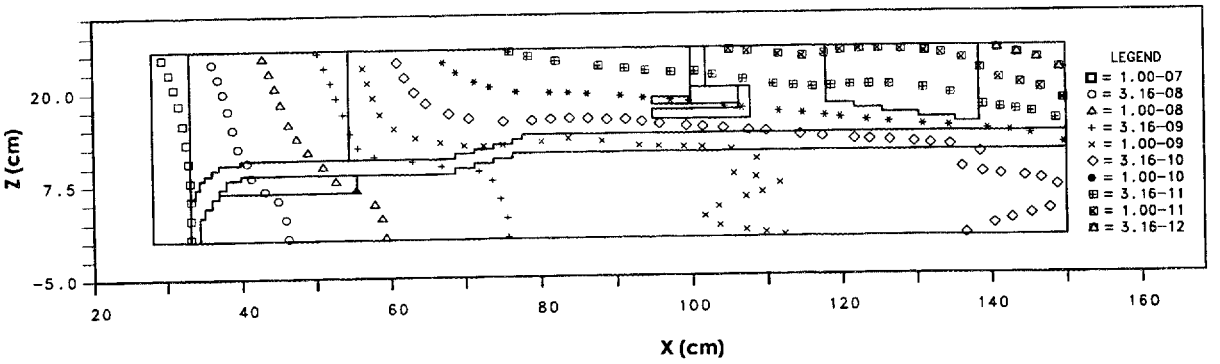

Figure E.10. Iso-plot of neutron dpa rate for HFIR HB-2 modified design for BOC conditions; annular beryllium insert; elevation view — vertical cut along beam tube axis.

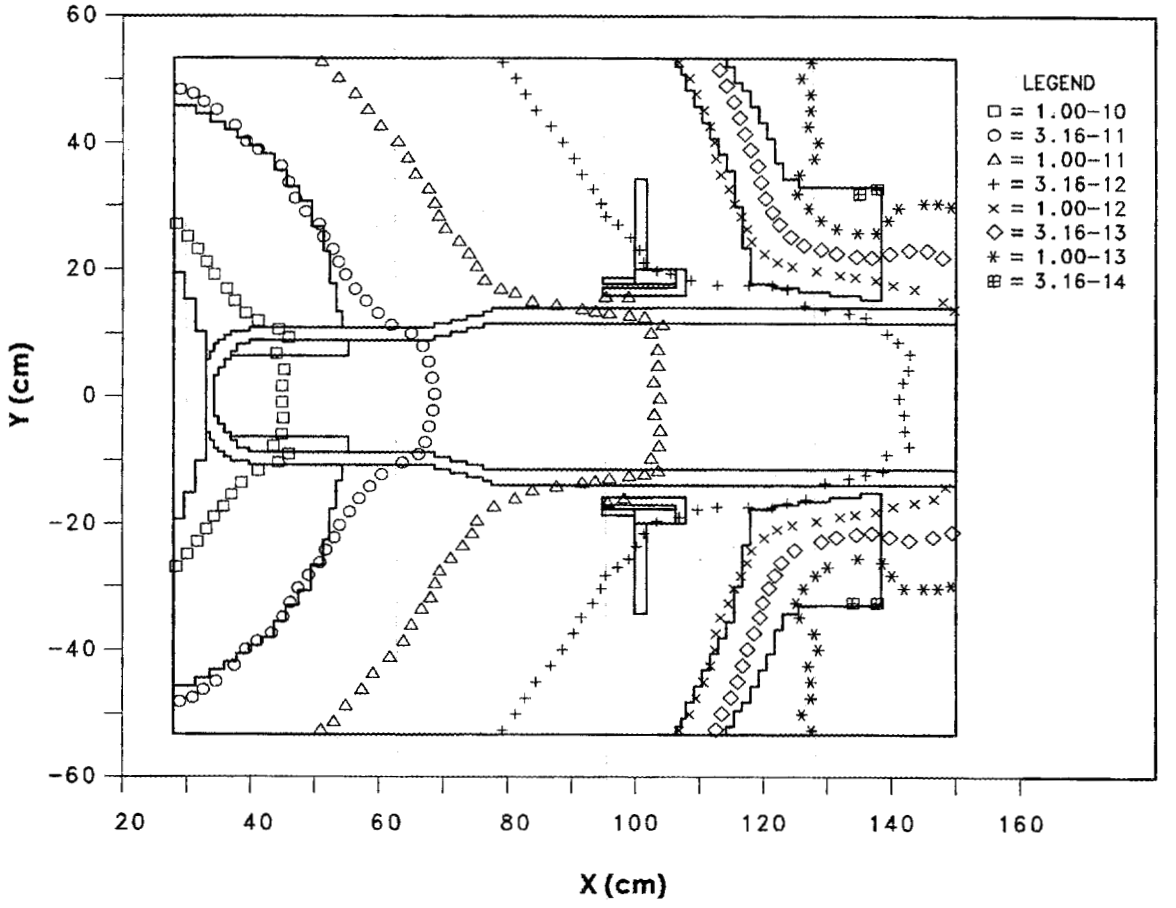

Figure E.11. Iso-plot of gamma dpa rate for HFIR HB-2 modified design for BOC conditions; annular beryllium insert; plan view — horizontal cut along beam tube axis.

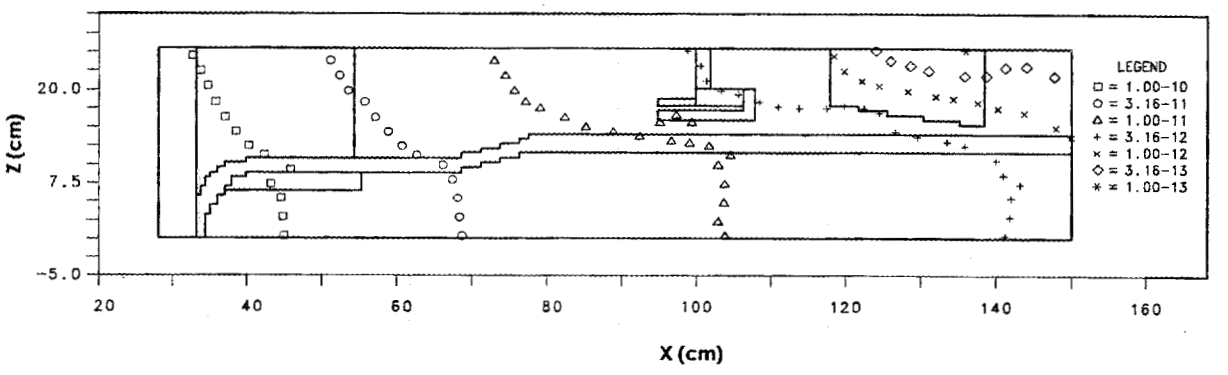

Figure E.12. Iso-plot of gamma dpa rate for HFIR HB-2 modified design for BOC conditions; annular beryllium insert; elevation view — vertical cut along beam tube axis.

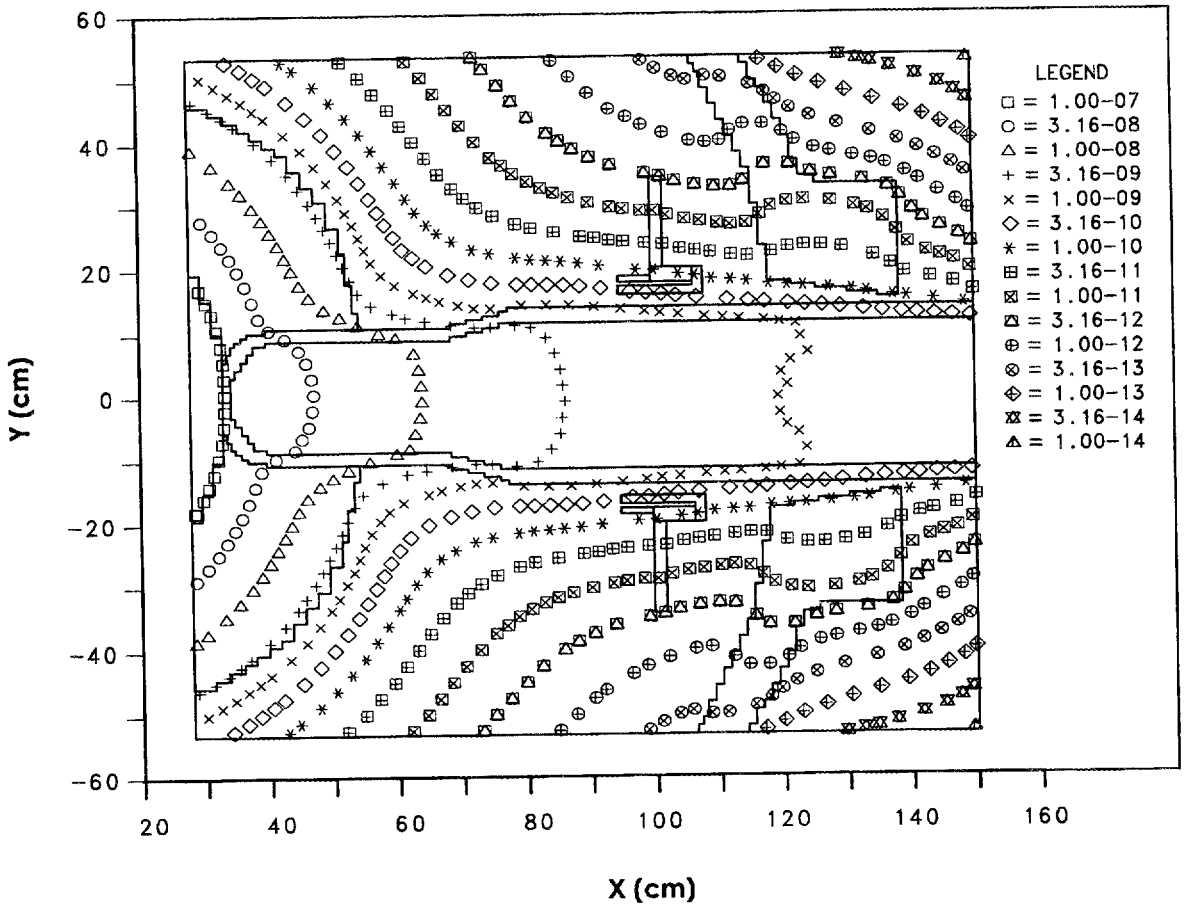

Figure E.13. Iso-plot of neutron dpa rate for HFIR HB-2 modified design for EOC conditions; no beryllium insert; plan view — horizontal cut along beam tube axis.

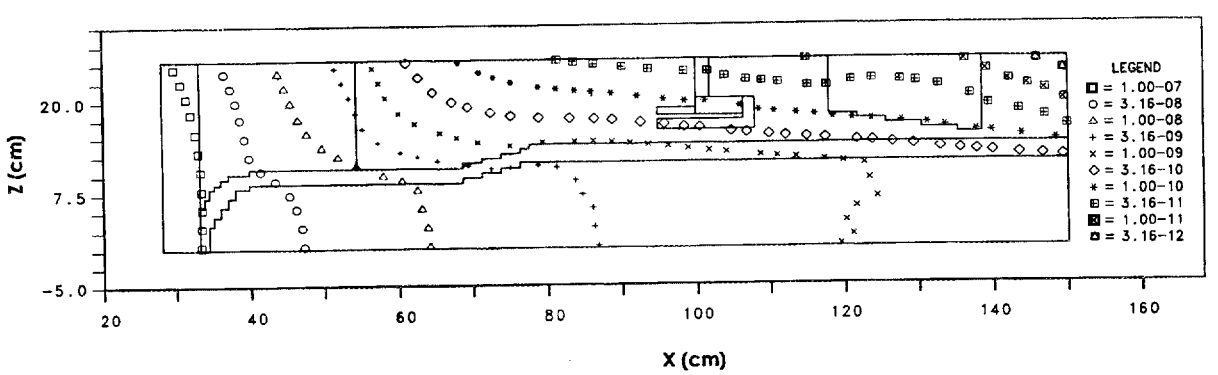

Figure E.14. Iso-plot of neutron dpa rate for HFIR HB-2 modified design for EOC conditions; no beryllium insert; elevation view — vertical cut along beam tube axis.

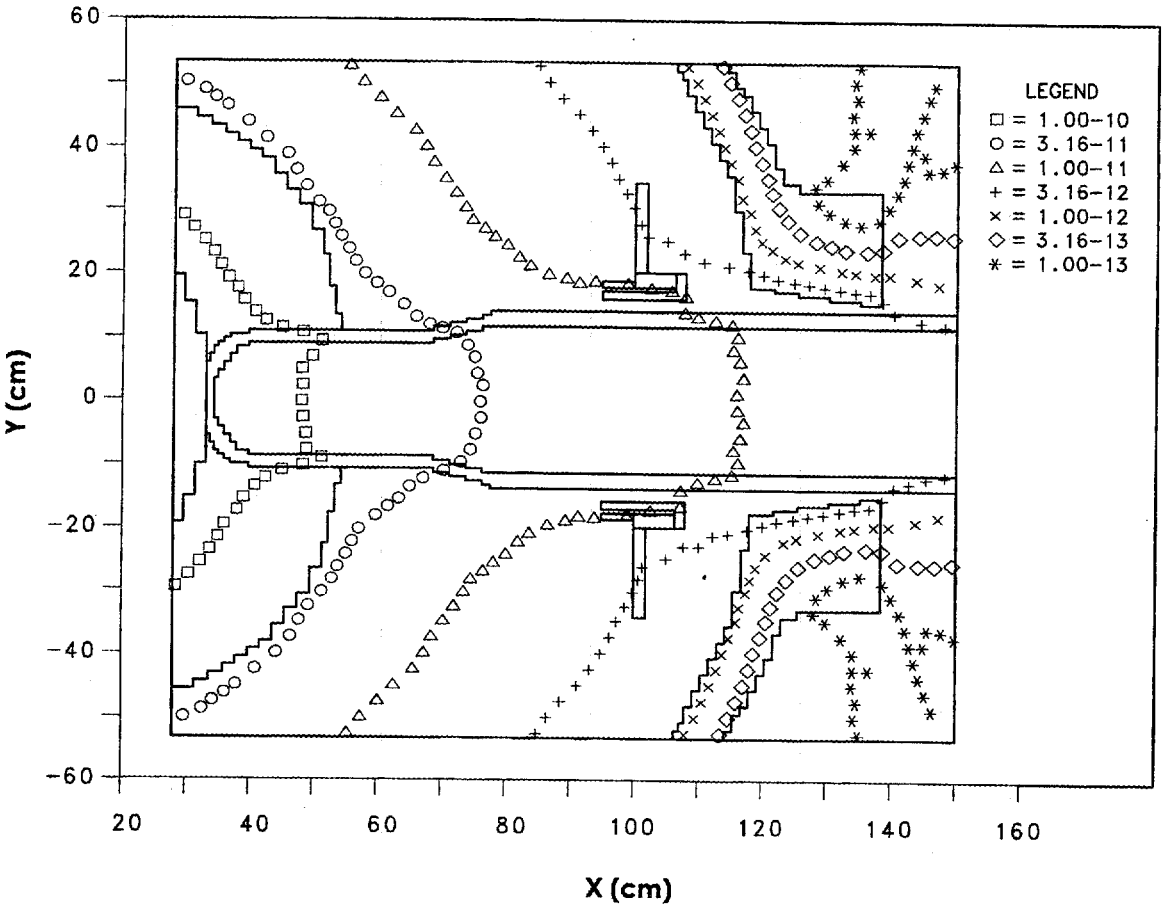

Figure E.15. Iso-plot of gamma dpa rate for HFIR HB-2 modified design for EOC conditions; no beryllium insert; plan view — horizontal cut along beam tube axis.

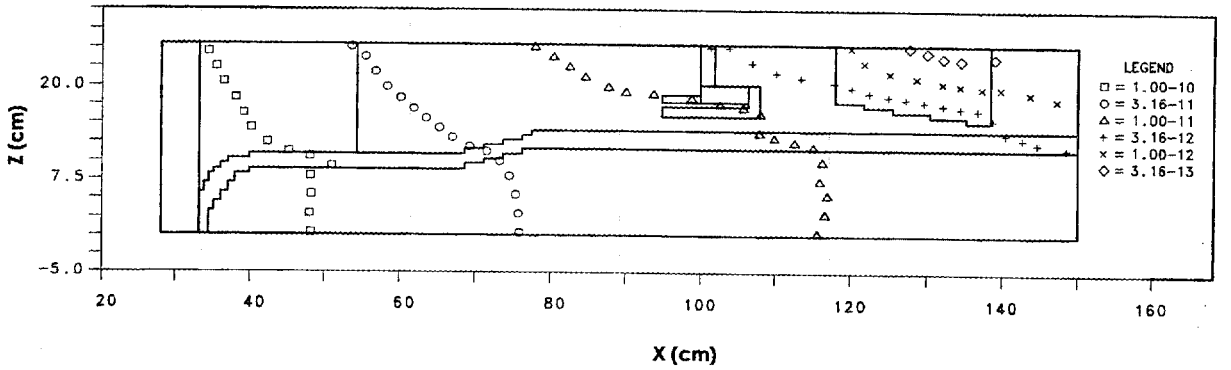

Figure E.16. Iso-plot of gamma dpa rate for HFIR HB-2 modified design for EOC conditions; no beryllium insert; elevation view — vertical cut along beam tube axis.

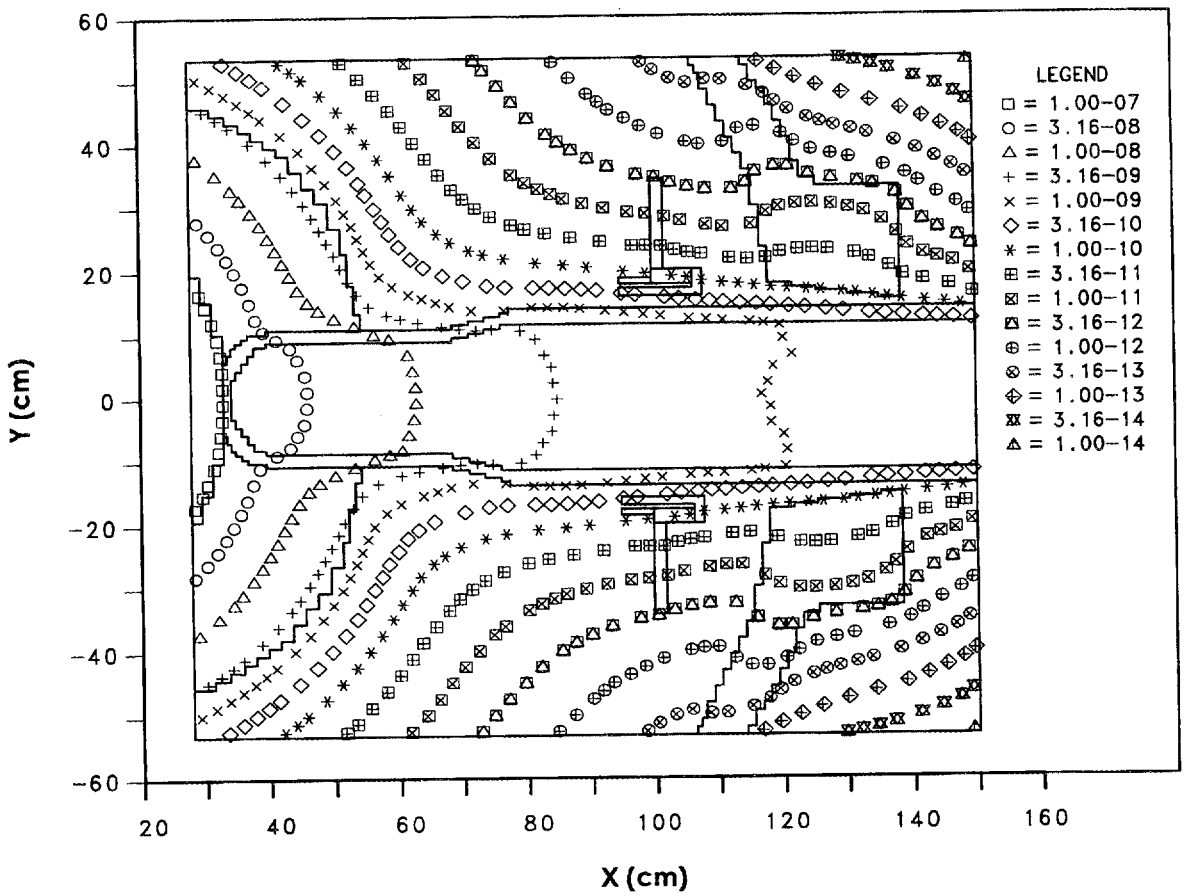

Figure E.17. Iso-plot of neutron dpa rate for HFIR HB-2 modified design for BOC conditions; no beryllium insert; plan view — horizontal cut along beam tube axis.

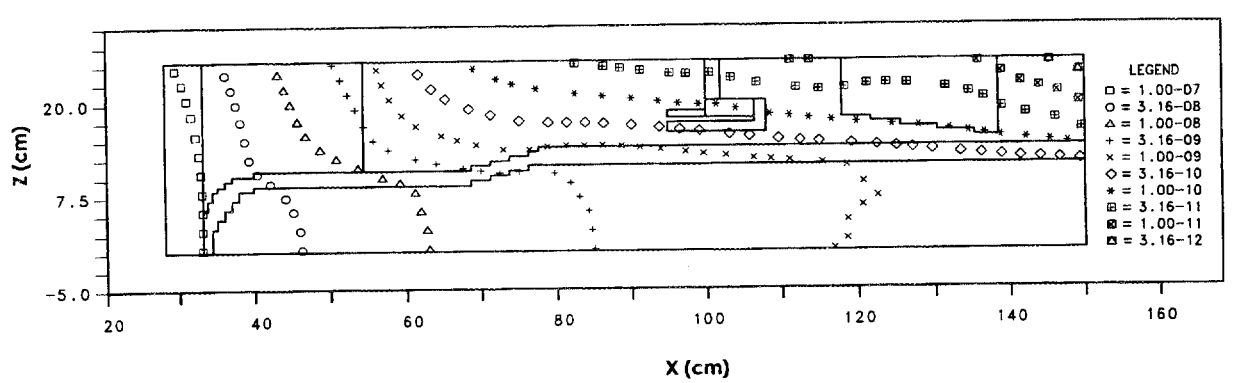

Figure E.18. Iso-plot of neutron dpa rate for HFIR HB-2 modified design for BOC conditions; no beryllium insert; elevation view — vertical cut along beam tube axis.

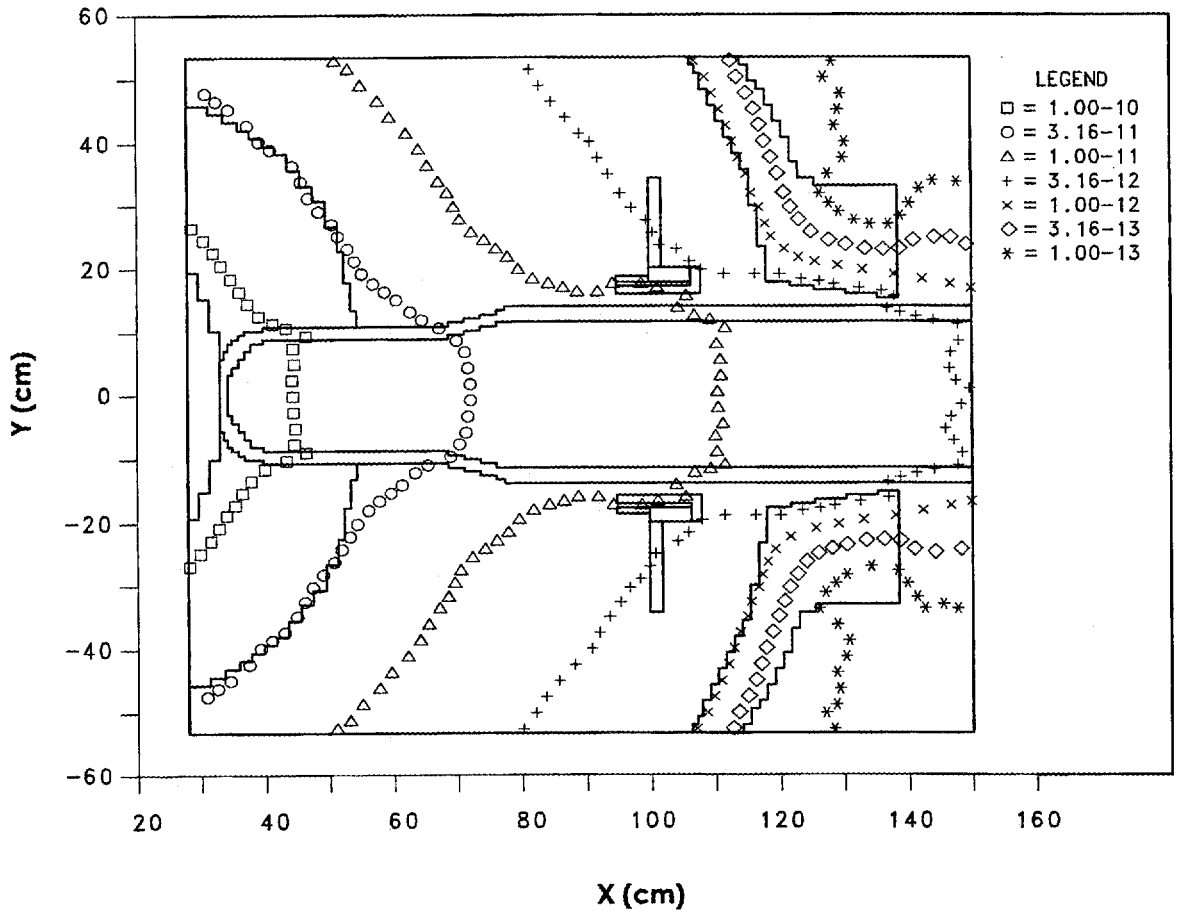

Figure E.19. Iso-plot of gamma dpa rate for HFIR HB-2 modified design for BOC conditions; no beryllium insert; plan view — horizontal cut along beam tube axis.

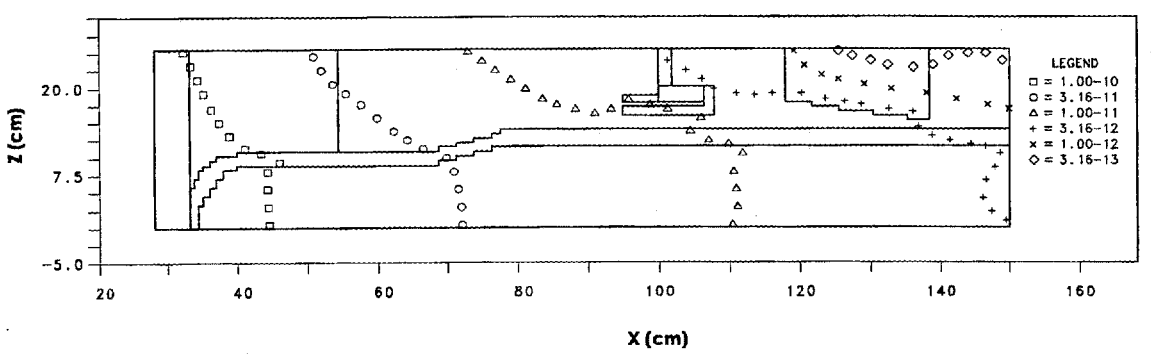

Figure E.20. Iso-plot of gamma dpa rate for HFIR HB-2 modified design for BOC conditions; no beryllium insert; elevation view — vertical cut along beam tube axis.

INTERNAL DISTRIBUTION

1-5. E. D. Blakeman
6. J. A. Bucholz
7. J. D. Bumgardner
8. S. J. Chang
9. R. D. Cheverton
10. R. E. Daniels
11. T. L. Dickson
12. M. B. Farrar
13. J. C. Gehin
14. R. W. Hobbs
15-19. J. R. Inger
20. D. T. Ingersoll
21. J. O. Johnson
22. M. W. Kohring
23. R. A. Lillie
24. M. A. Linn
25. L. D. Merryman
26. D. J. Newland
27. C. V. Parks
28. T. P. Powers
29. D. R. Reed
30. I. Remec
31. J. B. Roberto
32. J. E. Rushton
33. C. O. Slater
34. R. M. Stinnett
35. H. R. Vogel
36. M. R. Woods
37-38. RRD – DCC
39. Central Research Library
40. Laboratory Records

EXTERNAL DISTRIBUTION

41. Matt Huttmaker, Office of Nuclear Energy, NE-40-GTN, Department of Energy, Germantown, MD 20874-1290.
42. John O. Moore, ORNL Site Office, Department of Energy, Oak Ridge National Laboratory, Oak Ridge, TN 37831-6269.
43. George J. Malosh, ORNL Site Office, Department of Energy, Oak Ridge National Laboratory, Oak Ridge, TN 37831-6269.
44. Office of Scientific and Technical Information, Post Office Box 62, Oak Ridge, TN 37831 (2 copies).